nature biomedical engineering

ARTICLES

https://doi.org/10.1038/s41551-022-00847-9

Check for updates

Augmented lipid-nanoparticle-mediated in vivo genome editing in the lungs and spleen by disrupting Cas9 activity in the liver

Cory D. Sago[1,3,5], Melissa P. Lokugamage[1,4,5], David Loughrey[1], Kevin E. Lindsay[1], Robert Hincapie[2], Brandon R. Krupczak[1], Sujay Kalathoor[1], Manaka Sato[1], Elisa Schrader Echeverri[1], Jordan P. Fitzgerald[1], Zubao Gan[1], Lena Gamboa[1], Kalina Paunovska[1], Carlos A. Sanhueza[2], Marine Z. C. Hatit[1], M. G. Finn[2], Philip J. Santangelo[1] and James E. Dahlman[1]✉

Systemically delivered lipid nanoparticles are preferentially taken up by hepatocytes. This hinders the development of effective, non-viral means of editing genes in tissues other than the liver. Here we show that lipid-nanoparticle-mediated gene editing in the lung and spleen of adult mice can be enhanced by reducing Cas9-mediated insertions and deletions in hepatocytes via oligonucleotides disrupting the secondary structure of single-guide RNAs (sgRNAs) and also via their combination with short interfering RNA (siRNA) targeting Cas9 messenger RNA (mRNA). In SpCas9 mice with acute lung inflammation, the systemic delivery of an oligonucleotide inhibiting an sgRNA targeting the intercellular adhesion molecule 2 (ICAM-2), followed by the delivery of the sgRNA, reduced the fraction of ICAM-2 indels in hepatocytes and increased that in lung endothelial cells. In wild-type mice, the lipid-nanoparticle-mediated delivery of an inhibitory oligonucleotide, followed by the delivery of Cas9-degrading siRNA and then by Cas9 mRNA and sgRNA, reduced the fraction of ICAM-2 indels in hepatocytes but not in splenic endothelial cells. Inhibitory oligonucleotides and siRNAs could be used to modulate the cell-type specificity of Cas9 therapies.

Clustered regularly interspaced short palindromic repeat (CRISPR)-based gene editing systems have therapeutic promise[1], but their clinical use requires drug delivery[2,3]. Non-viral gene editing has been reported in adult animals in vivo after local administration of CRISPR therapies[4–6]. However, when administered systemically, editing often preferentially occurs in hepatocytes[7–13]. Unwanted hepatocyte delivery is a common problem for other nucleic acid therapies as well[14], and many nanoparticles preferentially deliver RNA to hepatocytes[15–17]. These data illustrate the potential impact of a programmable method to improve gene editing to other cell types.

To achieve non-hepatocyte drug delivery, scientists increase delivery to on-target cells by varying nanoparticle chemical structure, size or charge or by adding targeting ligands[18]. However, with few exceptions[19,20], off-target hepatocyte delivery remains unsolved, in large part because the structure of hepatic sinusoids promotes nanoparticle accumulation[21]. One alternative is to inhibit the activity of CRISPR-associated protein 9 (Cas9) in hepatocytes using oligonucleotides, thereby shifting the effective tropism of the nanoparticle away from the liver. For example, scientists reduced silencing mediated by *N*-acetylgalactosamine (GalNAc)-short interfering RNAs (siRNAs) using inhibitory oligonucleotides[22]. In another example, scientists included specialized anti-CRISPR proteins (Acrs) in adeno-associated viruses (AAVs), delivering one AAV expressing Cas9 and another AAV expressing the single-guide RNA (sgRNA) and an Acr. Acrs were designed with a microRNA (miRNA) binding site for miR-122, an miRNA highly expressed in the liver[23], which decreased Acr expression in the target tissue[24]. We envisioned exploiting hepatocyte delivery to inactivate sgRNA, SpCas9 (hereafter termed Cas9) messenger RNA (mRNA) or both with small inhibitory oligonucleotides termed iOligos. By delivering iOligos to hepatocytes, we reduced hepatocyte gene editing, thereby achieving preferential gene editing in the lungs and spleen.

Results

Antisense oligonucleotides for reducing Cas9 activity in vitro. Peptide-, protein- and small-molecule-based anti-CRISPRs that reduce gene editing in biochemical assays and in cell culture[25–28] led us to hypothesize that chemically modified anti-CRISPR oligonucleotides could reduce Cas9 editing in vivo. Researchers have previously used anti-CRISPRs that block interactions between pre-formed ribonucleoprotein (RNP) complexes and target DNA to reduce the gene editing (Fig. 1a). For example, the anti-CRISPR AcrIIC3 bound to NmeCas9/sgRNA complex in vitro decreased insertion and deletion (indel) formation in HEK293T cells[25]. In another example, AcrIIA4 reduced indel formation by >75% in K562 cells[26]. These advances are impactful but could be complemented in several ways. To begin with, whereas previous efforts destabilized pre-formed RNP complexes, it is unclear whether anti-CRISPRs will similarly inactivate drugs consisting of Cas9 mRNA and sgRNA packaged in the same lipid nanoparticle (LNP). We reasoned that, by exploiting the known secondary structure of the conserved region of the sgRNA, we could prevent RNP

[1]Wallace H. Coulter Department of Biomedical Engineering, Georgia Institute of Technology, Atlanta, GA, USA. [2]School of Chemistry and Biochemistry, Georgia Institute of Technology, Atlanta, GA, USA. [3]Present address: Beam Therapeutics, Atlanta, GA, USA. [4]Present address: Alloy Therapeutics, Lexington, MA, USA. [5]These authors contributed equally: Cory D. Sago, Melissa P. Lokugamage. ✉e-mail: james.dahlman@bme.gatech.edu

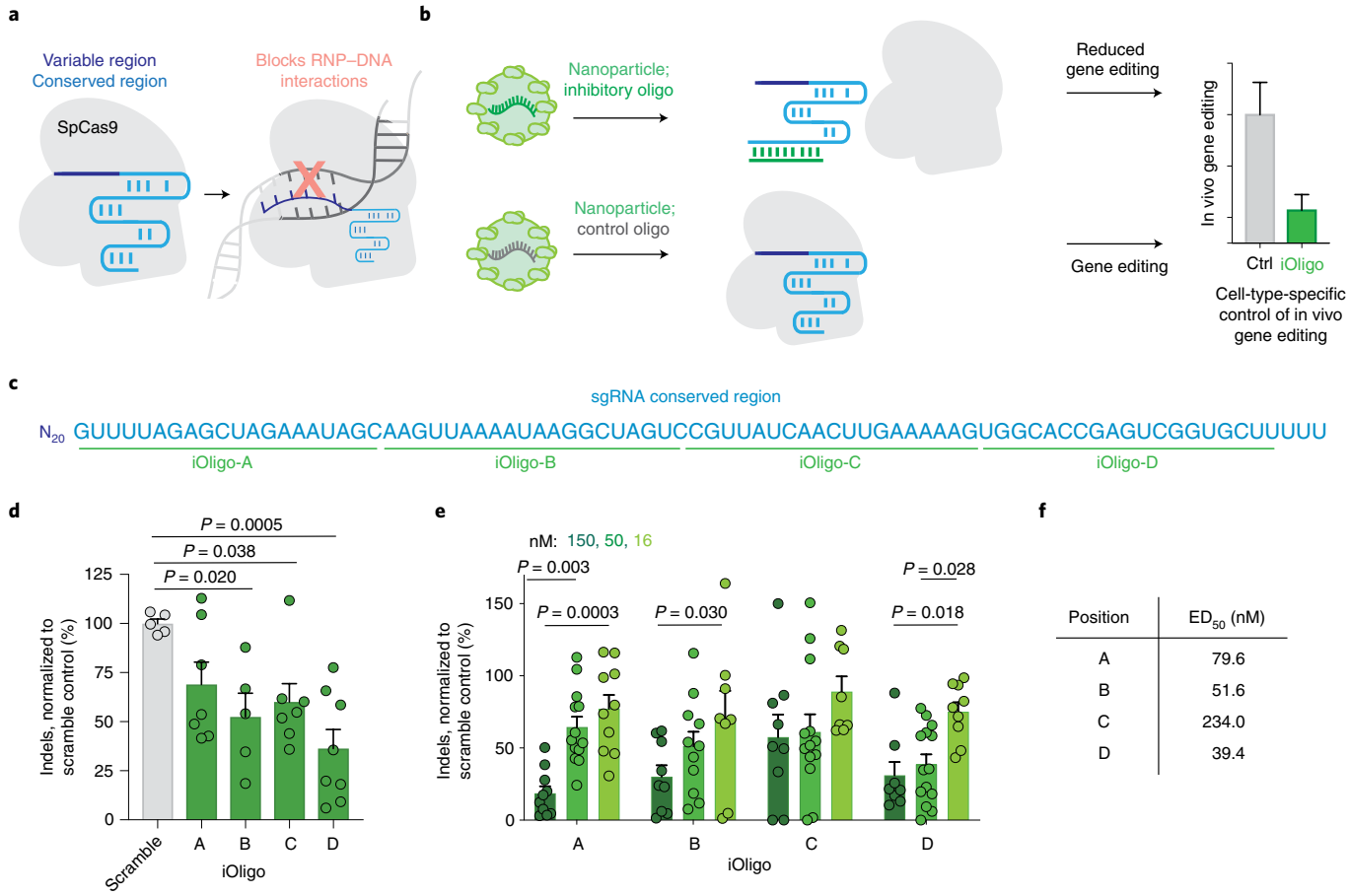

Fig. 1 | Synthetic antisense oligonucleotides termed iOligos reduce Cas9 activity in cell culture. a, Cas9 and sgRNA form an RNP that binds to and edits DNA. Previously described anti-CRISPRs block interactions between RNPs and DNA. **b**, A proposed mechanism of iOligo-mediated inhibition of gene editing. By complexing with the conserved region of the sgRNA and disrupting its secondary structure, iOligos prevent gene editing. **c**, iOligos were tiled in the conserved region of the sgRNA backbone; N_{20}, non-conserved sequence that varies with targeted DNA. **d**, Indel percentage in Cas9-expressing cells after treatment with 50 nM iOligos or a control; iOligos prevented indel formation in cell culture when transfected 4 h before sgRNA. *P* values shown relative to scramble control, one-way analysis of variance (ANOVA), average ± s.e.m., $n = 5$–8. **e**, Each of the four iOligos reduced indel formation in a dose-dependent manner; *P* values shown relative to scramble control, one-way ANOVA, average ± s.e.m., $n = 8$–14. **f**, Calculated iOligo dose required to inhibit indel formation by 50%. ED_{50}, median effective dose. All replicates are biological.

complex formation (Fig. 1b), a mechanism that could be useful for mRNA-based therapies.

We also reasoned that an oligonucleotide anti-CRISPR could be advantageous for several reasons. First, oligonucleotides are well tolerated in humans[29–31]. Second, scientists have identified chemical modifications that increase oligonucleotide stability and reduce immunogenicity[32]. Third, it is possible to deliver oligonucleotides to hepatocytes using FDA-approved LNPs or GalNAc. Fourth, oligonucleotide delivery in non-human primates has been achieved in monocytes[33] and endothelial cells[34], suggesting that iOligos could reduce gene editing in other cell types.

We first investigated whether iOligos inhibited Cas9 activity. We tiled four iOligo sequences across the conserved region of sgRNA[35] (Fig. 1c and Supplementary Fig. 1a). Each iOligo was chemically modified at every position with 2′-*O*-methyl ribose and phosphorothioates to increase stability, reduce immunogenicity and increase affinity of the iOligo for target RNA[36]. We performed initial experiments in immortalized aortic endothelial cells (iMAECs)[37] transduced with lentivirus to stably express Cas9 (hereafter termed Cas9-iMAECs). Using Lipofectamine 2000, we transfected iOligos at a dose of 50 nM into Cas9-iMAECs. Four hours later, we transfected the same cells with 16 nM sgRNA targeting ICAM-2 (intercellular adhesion molecule 2, sgICAM-2). This sgICAM-2 sequence was chemically modified to reduce immunostimulation and increase stability[38] (Supplementary Fig. 1b). Seventy-two hours later, we isolated genomic DNA from cells and quantified indels using Tracking of Indels by Decomposition (TIDE)[39]. Compared with a scrambled oligonucleotide with the same length and chemical modifications, which acted as a control, all four iOligos reduced Cas9-mediated indels in a mostly dose-dependent manner (Fig. 1d–f). We selected iOligo-D (hereafter termed iOligo), which targeted the 3′ end of the sgRNA, for further studies. Given that these results were generated in Cas9-iMAECs, we then investigated whether iOligo reduced indels when Cas9 was delivered transiently via mRNA. We transfected iOligo at a dose of 16 nM and then transfected wild-type iMAECs with 300 ng Cas9 mRNA and 16 nM sgICAM-2. Once again, iOligo reduced indel formation. By varying the time between iOligo administration and Cas9/sgRNA administration, we found that iOligo was most effective when delivered 2 h before the mRNA and sgRNA (Supplementary Fig. 1c). These results suggest that synthetic, chemically modified oligonucleotides reduced Cas9 gene editing in murine cells.

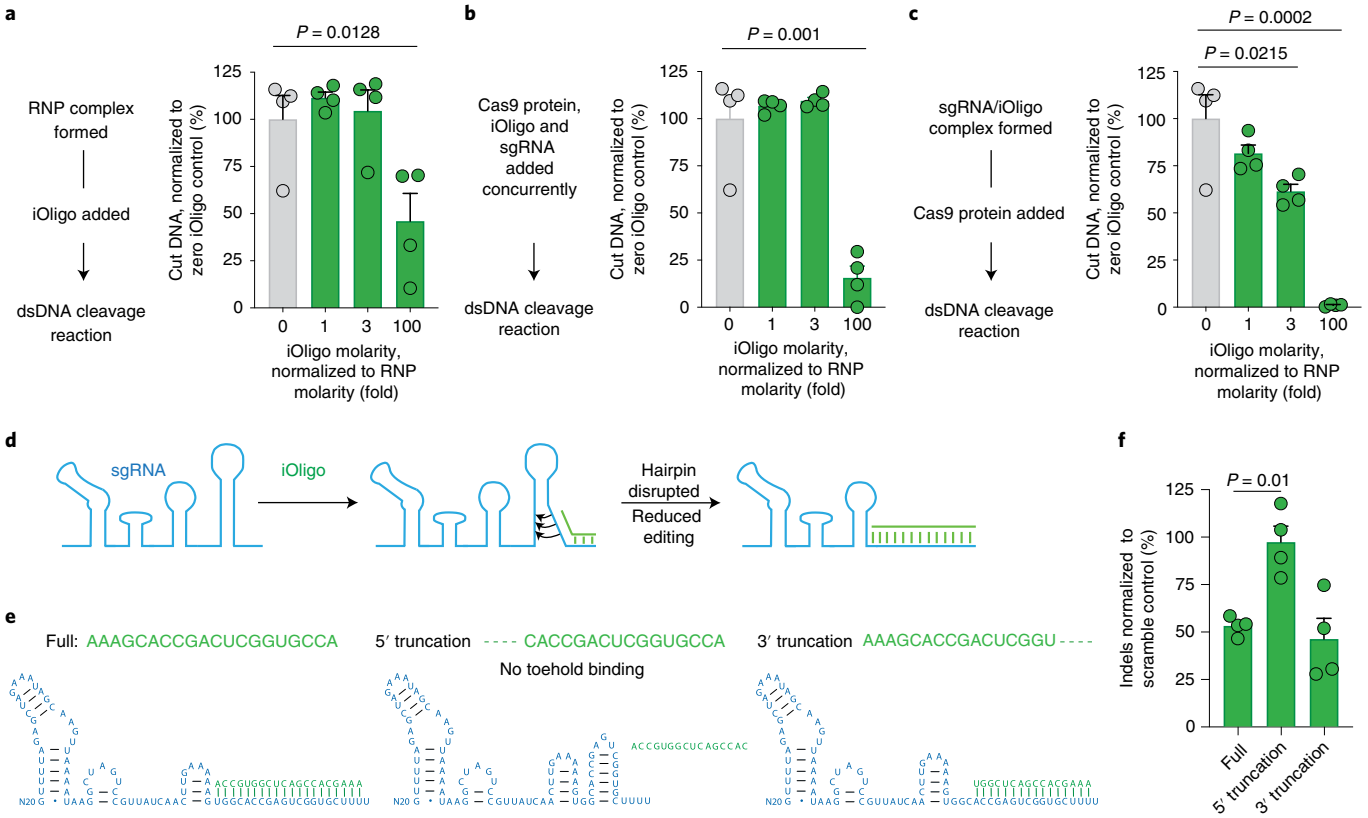

Fig. 2 | iOligo reduces gene editing by interacting with sgRNA. a–c, DNA cleavage efficiency in the presence of iOligo normalized to cleavage with just the pre-formed Cas9 RNP complex. iOligo was added after the sgRNA/Cas9 complex was allowed to form (**a**) to the sgRNA at the same time as the Cas9 protein (**b**) or the sgRNA/iOligo complex was allowed to form first before the Cas9 protein was added (**c**). *P* values shown relative to RNP complex control, one-way ANOVA, average ± s.e.m., $n = 4$. **d**, Schematic of the mechanism. The iOligo is designed to be complementary to the 3′ end of the sgRNA terminator hairpin. When present, iOligo binds to the terminator sequence, preventing Cas9 protein binding and reducing DNA editing. **e**, The linear region of the polyU tail of the terminator structure is required as a three-nucleotide toehold to mediate a strand displacement reaction and facilitate iOligo binding. **f**, Normalized indels in Cas9-expressing cells after treatment with full-length and truncated versions of the iOligo. *P* value shown relative to scramble control, one-way ANOVA, average ± s.e.m., $n = 4$. All replicates are biological.

iOligo reduces gene editing by interacting with guide RNAs. We then characterized the biochemical mechanism by which iOligo reduced gene editing by evaluating whether iOligo disrupted already-formed Cas9/sgRNA RNP complexes. We combined sgRNA and Cas9 protein at an equimolar concentration to form RNP complexes, added 1 µM pre-formed RNP complexes to 100 nM target DNA substrate and then quantified DNA cutting 1 h later. In the control condition (0 µM iOligo), we observed DNA cutting as expected. When 1 µM or 3 µM iOligo was added after RNP complex formation, DNA cutting was unchanged (Fig. 2a). We found that 100 µM iOligo was required to reduce DNA cutting, indicating that iOligo did not readily disrupt pre-formed RNP complexes[40]. We repeated these experiments adding iOligo at the same time as the Cas9 protein so that the two molecules competed (Fig. 2b). Once again, 100 µM iOligo was required to statistically reduce DNA cutting. We then pre-formed the sgRNA/iOligo complex before adding the Cas9 protein, which may be similar to LNP-mediated Cas9 mRNA and sgRNA delivery (Fig. 2c). In this case, 3 µM iOligo inhibited DNA cleavage, suggesting that iOligo efficacy increases if it binds sgRNA before an RNP complex has formed. We then evaluated whether iOligo prevented RNP complex formation using an electrophoretic mobility shift assay (EMSA). We incubated 1.5 pmol sgRNA with 1.5 pmol Cas9 protein (RNP) or 5 pmol iOligo to form a complex and then attempted to disrupt the complex by adding the third molecule. These results provided additional evidence that iOligo prevents RNP complex formation by binding the sgRNA but does not readily dissociate RNP complexes after they form (Supplementary Fig. 2a).

We investigated how sgRNA secondary structure affected iOligo inhibition in cells. We designed iOligo to bind the stem-loop structure as well as the polyU toehold at the 3′ terminus of the sgRNA (Fig. 2d). We hypothesized that iOligo worked, in part, by disrupting sgRNA secondary structure via a toehold. On the basis of previous toeholds[41], we reasoned that binding the linear region of the sgRNA tail was required to initiate an RNA–RNA strand displacement (Fig. 2e). During toehold-mediated strand displacement[41], a small, linear, unstructured toehold region is exposed, which seeds the interaction with the invading complementary iOligo; the polyU at the 3′ terminus of the sgRNA acts as this toehold region. We, therefore, measured indel formation in Cas9-iMAECs pre-treated with iOligo mutants containing four nucleotide truncations from the 5′ or 3′ end. We transfected Cas9-iMAECs with 50 nM iOligo and then 4 h later with 16 nM sgICAM-2. Three days later, we quantified ICAM-2 indel percentage. When compared with control cells that were not treated with iOligo, we found that the full-length iOligo control reduced indel formation. Consistent with our toehold hypothesis, we observed that the iOligo with 5′ truncations no longer prevented indel formation, whereas the iOligo with 3′ truncations did prevent indel formation (Fig. 2f).

To investigate whether this toehold mechanism applied to other RNA-guided nucleases, we used our CRISPR–Cas9 results to rationally design iOligo inhibitors targeting CRISPR–Cas12a[42]. As a control, we used a 41-nucleotide (nt) oligonucleotide complementary to the entire CRISPR RNA (crRNA), including the region that varies with the targeted gene, thereby inhibiting Cas12a[43]; by contrast, iOligo targeted the conserved region of the crRNA. We transfected HEK293T cells with a previously reported[44] crRNA targeting green fluorescent protein (GFP, crGFP; Extended Data Fig. 1a) and a chemically modified mRNA encoding Cas12a. We first tested the 41-nt sequence, and we found it reduced indels compared with a scramble oligonucleotide, as previously reported[45] (Extended Data Fig. 1b,c). Our proposed mechanism requires a 5′ toehold that disrupts the secondary structure of the crRNA (Extended Data Fig. 1d). We designed three truncated iOligo variants to test this mechanism. Variant one did not include a toehold but disrupted secondary structure. Variant two included a toehold but did not disrupt crRNA secondary structure. Variant three included a toehold and disrupted secondary structure (Extended Data Fig. 1e). As hypothesized, variants one and two did not inhibit Cas12a-mediated gene editing, whereas variant three did so as efficiently as the 41-nt fully complementary control (Extended Data Fig. 1f,g).

We then evaluated whether chemical modifications altered the efficacy of iOligo targeting Cas9 sgRNA. We administered 50 nM iOligo with fewer modifications to Cas9-iMAECs (Extended Data Fig. 2a). The control iOligo (that is, fully modified) outperformed iOligo with fewer modifications (Extended Data Fig. 2b). These results suggest that iOligo-mediated inhibition is not caused by RNase H-mediated sgRNA degradation, consistent with the fact that 2′-*O*-methyl modifications prevent RNase H activity[46]. Fully modified iOligo with 2-methoxyethyl modifications did not increase the efficacy compared with iOligo with 2′-*O*-methyl modifications (Extended Data Fig. 2c,d). This also suggests that iOligo works via an RNase-independent mechanism, as neither 2′-*O*-methyl nor 2-methoxyethyl modifications are tolerated by RNase H in the non-wing portion of the antisense oligonucleotide (ASO)[46]. Further work is required to understand whether iOligo-mediated disruption of gene editing is truly RNAse independent.

We investigated whether iOligo could programmably control gene editing in the liver, lung and spleen. The experimental details of all in vivo experiments are listed (Supplementary Fig. 3a–c and Supplementary Table 1). First, we reduced gene editing in hepatocytes (Fig. 3a). We created hepatocyte-targeting LNPs by mixing C_{14}PEG2000, cholesterol, 1,2-distearoyl-sn-glycero-3-phosphocholine (DSPC) and the ionizable lipid cKK-E12 (ref. [16]) in a microfluidic device[47]. This LNP delivers siRNA, sgRNA and mRNA to hepatocytes in vivo[9,16], and we named it LNP-Hepat for simplicity[48] (Fig. 3b). We formulated LNP-Hepat to carry iOligo or, as a control, a scrambled oligonucleotide sequence. Separately, we formulated LNP-Hepat to carry chemically modified sgGFP. We injected mice that express Cas9-GFP under a ubiquitous CAG promoter[49] with iOligo or with the control oligonucleotides. Two hours later, we injected the same mice with sgGFP. Five days later, we euthanized the mice, isolated $CD31^{-}CD45^{-}$hepatocytes using fluorescence-activated cell sorting (FACS) and quantified sgGFP indels. Compared with control mice injected with the control oligonucleotide, the indel percentages decreased by 58% in iOligo-treated mice (Fig. 3c). We observed no measurable changes in aspartate aminotransferase (AST) levels after administering iOligo compared with phosphate-buffered saline (PBS)-treated control mice (Supplementary Fig. 3d).

We then evaluated whether iOligo could mediate organ-specific reductions in gene editing by reducing gene editing in hepatocytes without reducing gene editing in the lungs (Fig. 3d). We formulated LNP-Hepat with either iOligo or the scrambled oligonucleotide and then intravenously injected into Cas9-GFP mice. Separately, we formulated sgGFP into LNPs made from the lipid 7C1 and C_{14}PEG2000 to deliver RNA to lung endothelial cells[50], which we named LNP-Lung (Fig. 3e). Five days after the injections, we isolated hepatocytes as well as $CD31^{+}CD45^{-}$ lung endothelial cells using FACS and quantified sgGFP indels. Compared with hepatocytes isolated from mice pre-treated with the scramble control, hepatocytes isolated from mice treated with iOligo exhibited fewer indels. By contrast, indels in lung endothelial cells remained unchanged (Fig. 3f). In the in vivo experiments described above, iOligo did not lead to weight loss (Supplementary Fig. 3c). We measured editing in other non-targeted organs in animals injected with LNP-Lung. We observed low levels of editing in spleen T cells and endothelial cells and no editing in spleen B cells or lung immune cells (Supplementary Fig. 3e). In addition, we quantified whole-liver editing and observed reduced editing in hepatocytes treated with iOligo (Supplementary Fig. 3f).

siRNA regulation of Cas9 expression can alter gene editing in vitro and in vivo. Since iOligo targets sgRNA, we reasoned that an orthogonal approach targeting Cas9 mRNA could further reduce gene editing in hepatocytes. We hypothesized that, by rationally designing a Cas9 mRNA to be sensitive to a previously validated[51] siRNA targeting GFP (siGFP), we could pre-treat animals with siGFP delivered to hepatocytes, thereby reducing Cas9 protein production and subsequent gene editing (Fig. 4a). We first designed a Cas9 mRNA that could be degraded in vivo with an appropriate input signal. Specifically, we in vitro transcribed an N1-methyl-pseudouridine containing Cas9 mRNA with five identical binding sites for siGFP cloned into its 3′ untranscribed region (UTR) (Supplementary Fig. 4a). Using Lipofectamine 2000, we transfected iMAECs with siGFP or a previously validated and chemically modified siRNA that targeted luciferase, which we termed siControl (Supplementary Fig. 4b). Ten hours later, we transfected cells with Cas9 mRNA and sgICAM-2. A 14 h time point was selected to maximize siRNA RISC (RNA-induced silencing complex) loading[52,53]. When compared with cells pre-treated with 20 nM siControl, cells pre-treated with 20 nM siGFP produced 65% less Cas9 protein, quantified by flow cytometry mean fluorescence intensity (MFI, Fig. 4b). Indels in cells treated with siGFP also decreased compared to cells treated with siControl (Fig. 4c). When we held the siRNA dose constant at 20 nM, the potency of the siRNA-mediated indel reduction improved as the amount of Cas9 mRNA transfected into cells decreased, as expected (Fig. 4d).

We then investigated whether Cas9 mRNA degradation led to cell-type-specific control of gene editing in vivo using additional animal models. First, we intravenously injected wild-type mice with siControl or siGFP formulated into LNP-Hepat. Fourteen hours later, we injected the same mice with LNP-Hepat carrying Cas9 mRNA as well as a chemically modified sgRNA targeting ICAM-2 (ref. [38]; Fig. 4e). Five days later, we isolated hepatocytes using FACS and quantified ICAM-2 indels. Compared with hepatocytes isolated from mice treated with siControl, hepatocytes isolated from mice treated with siGFP had fewer indels (Fig. 4f). We then evaluated whether siGFP reduced hepatocyte editing without reducing editing in the spleen (Fig. 4g). Fourteen hours after injecting wild-type mice with siControl or siGFP, we injected mice with an LNP with a well-characterized biodistribution profile that facilitates gene editing in hepatocytes and splenic endothelial cells[38], named LNP-Spleen (Fig. 4h). Five days later, we isolated hepatocytes and $CD31^{+}CD45^{-}$ splenic endothelial cells using FACS. Hepatocyte indels decreased significantly, whereas splenic endothelial cell indels did not (Fig. 4i).

We repeated this approach using luciferase mRNA. We first designed and transcribed a chemically modified mRNA encoding luciferase with 3′ UTR sequence containing five siGFP-binding sites, identical to the approach used for the Cas9 mRNA (Extended Data Fig. 3a). We pre-treated iMAECs with 20 nM control siRNA

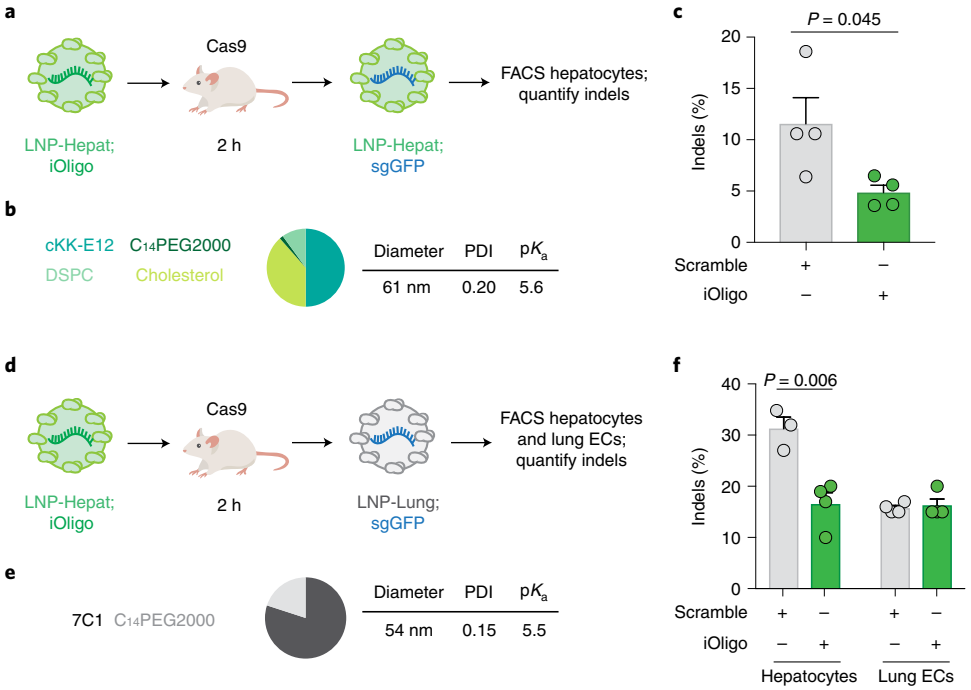

Fig. 3 | iOligo controls systemic gene editing in vivo. a, Mice that constitutively express Cas9 were injected with LNP-Hepat carrying iOligos or a scrambled oligonucleotide control. Two hours later, mice were injected with LNP-Hepat carrying sgRNA. **b**, LNP-Hepat chemical composition and biophysical traits. **c**, Indel percentages in hepatocytes isolated by FACS. *P* value shown, two-tailed *t*-test, average ± s.e.m., $n = 4$. **d**, Mice that constitutively express Cas9 were injected with LNP-Hepat carrying iOligo or a scrambled oligonucleotide control. Two hours later, mice were injected with LNP-lung carrying sgRNA. **e**, LNP-Lung chemical composition and biophysical traits. **f**, Indel percentages in hepatocytes and lung endothelial cells (ECs) isolated by FACS. Indels decreased in hepatocytes but remained constant in lung endothelial cells. *P* value shown, one-way ANOVA, average ± s.e.m., $n = 3$–4. All replicates are biological. 7C1, an oligomer–lipid conjugate; ECs, endothelial cells; PDI, polydispersity index.

targeting ICAM-2 (siICAM-2) or siGFP and then administered varying amounts of luciferase mRNA. We used siICAM-2 as a control siRNA, because siLuciferase, which served as our siControl in the Cas9 mRNA experiments, was not an appropriate control for luciferase mRNA. Luminescence decreased by up to 79% in cells pre-treated with siGFP relative to cells treated with siICAM-2 (Extended Data Fig. 3b). To test whether this approach reduced luciferase in vivo, we injected mice with LNP-Hepat containing siGFP or siICAM-2, waited 14 h and then injected the mice with LNP-Hepat carrying luciferase mRNA (Extended Data Fig. 3c). Six hours later, we administered luciferin to mice, isolated the liver and quantified luminescence. Compared with mice treated with siICAM-2, mice treated with siGFP generated 74% less luminescence (Extended Data Fig. 3d).

We reasoned that combining iOligo (which targets sgRNA) and siRNA (which targets Cas9 mRNA) would reduce editing in vivo (Fig. 5a). We tested this in wild-type mice using two additional animal models. First, we intravenously injected mice with LNP-Hepat carrying siGFP, and then, 14 h later, we injected the mice with LNP-Hepat carrying iOligo. Two hours later, we injected the mice with Cas9 mRNA and sgRNA formulated in LNP-Spleen. We compared four groups of mice, including groups treated with a control oligo (in place of iOligo) or, alternatively, siControl (in place of siGFP). Combining iOligo and siGFP potently reduced editing in hepatocytes (Fig. 5b) without reducing editing in splenic endothelial cells (Fig. 5c). We quantified the ratio of indels in splenic endothelial cells and hepatocytes and found the splenic endothelial cell/hepatocyte ratio to be higher when iOligo and siGFP were combined, relative to iOligo or siGFP individually (Fig. 5d). We measured off-target editing in other organs for LNP-Spleen. We observed low off-target editing in T cells, B cells and lung endothelial cells and no editing in lung immune cells (Supplementary Fig. 5a). In addition, we quantified whole-liver editing and observed reduced editing in hepatocytes treated with iOligo (Supplementary Fig. 5b). The combination of iOligo and siUTR did not lead to mouse weight loss (Supplementary Fig. 3c).

Second, we evaluated whether combining iOligo and siGFP reduced indels in hepatocytes when the inhibitory molecules were delivered using GalNAc instead of LNP-Hepat (Fig. 5e). LNP-Hepat has been used to deliver RNA to hepatocytes in non-human primates and is licensed for clinical use[16]. GalNAc has been used to deliver siRNA to hepatocytes in patients[54]. We conjugated siGFP (Supplementary Fig. 4b) with alternating 2′-fluoro- and 2′-*O*-methyl modifications to resist nuclease degradation (hm-siGFP) to a previously described asialoglycoprotein receptor (ASGPR) conjugate[55] using click chemistry (Supplementary Fig. 6). Specifically, we reacted hm-siGFP modified with an alkyne on the 5′ end of the sense strand with excess azido-ASGPR-trimer ligand. After verifying conjugation using mass spectrometry, we annealed the antisense siRNA to the ASGPR–hm-siGFP conjugate and confirmed the annealing with an agarose gel (Supplementary Fig. 7). The ASGPRL–iOligo was conjugated similarly using an alkyne on the 5′ end (Supplementary Fig. 8). We subcutaneously injected wild-type mice with 20 mg kg^{-1} siGFP conjugated to GalNAc. Twelve hours later, we subcutaneously injected mice with 20 mg kg^{-1} iOligo conjugated to GalNAc. Notably, GalNAc–siRNA conjugates have been reported to be well tolerated in mice at doses as high as 100 mg kg^{-1} (ref. [56]). Two hours later, we injected mice with LNP-Spleen containing sgICAM-2 and the siGFP-sensitive Cas9 mRNA. Five days after the LNP-Spleen injection, we isolated hepatocytes and splenic endothelial cells and quantified indel percentages. Hepatocyte indels showed a slight decrease, whereas splenic endothelial cell indels showed no decrease (Fig. 5f,g).

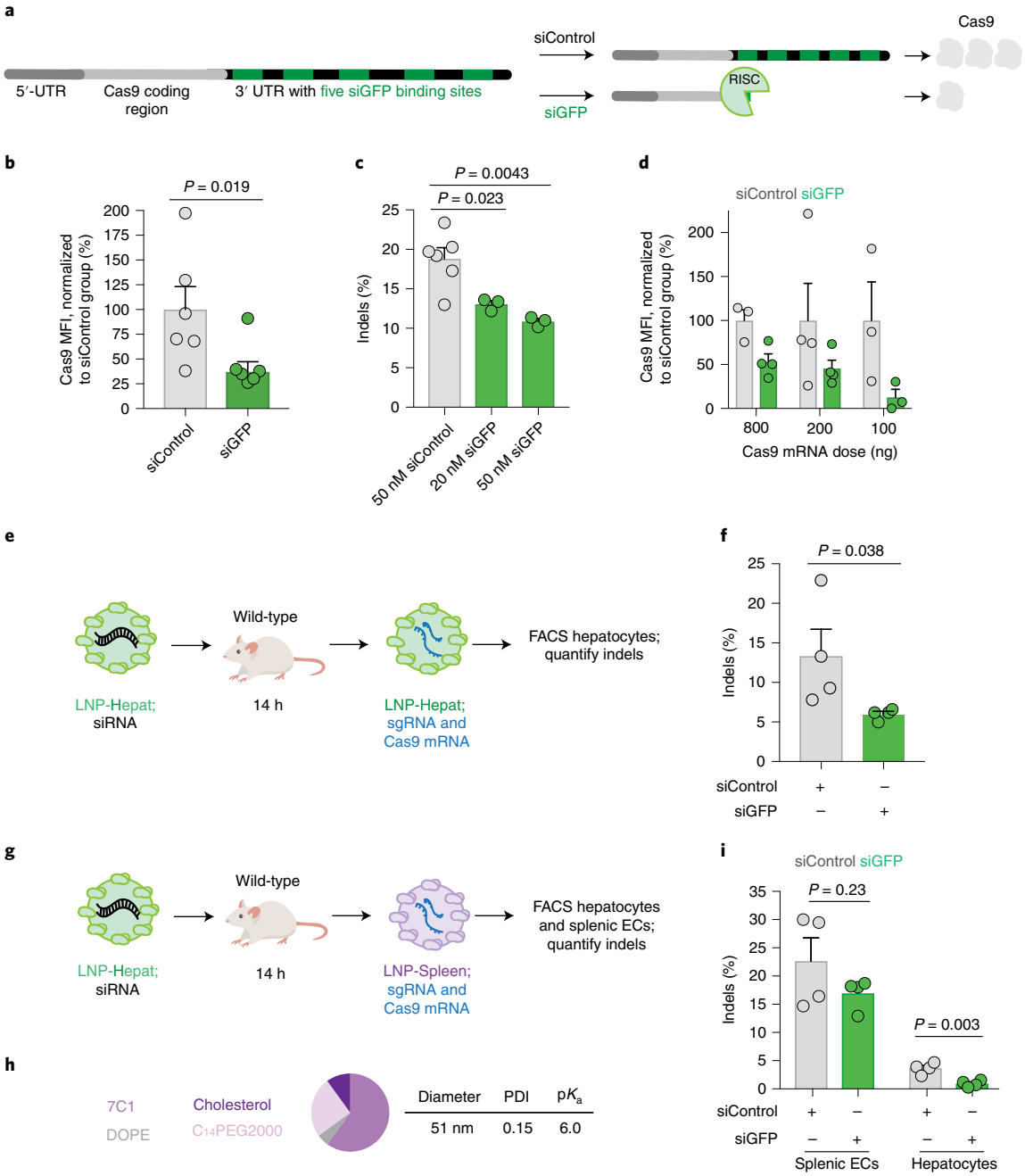

Fig. 4 | siRNA-mediated reduction of Cas9 expression controls gene editing in vitro and in vivo. a, mRNA encoding for Cas9 was designed to be sensitive to siRNA degradation by including five siGFP-binding sites in the 3′ UTR. **b**,**c**, Cas9 protein expression (**b**) and ICAM-2 indels (**c**) following treatment of cells with siGFP or siControl and then Cas9 mRNA and sgICAM-2 . *P* values shown, one-way ANOVA, average ± s.e.m., $n = 3$–6. **d**, Pre-treating cells with siGFP decreased Cas9 protein production in a dose-dependent manner, average ± s.e.m., $n = 3$–4. **e**, Wild-type mice were injected with LNP-Hepat carrying siControl or siGFP. Fourteen hours later, mice were injected with LNP-Hepat carrying Cas9 mRNA and sgICAM-2. **f**, Normalized indel percentage in hepatocytes after treatment with siControl or siGFP. *P* value shown, one-tailed *t*-test, average ± s.e.m., $n = 4$. **g**, Wild-type mice were injected with siControl or siGFP carried by LNP-Hepat. Fourteen hours later, mice were injected with LNP-Spleen carrying Cas9 mRNA and sgICAM-2. **h**, LNP-Spleen chemical composition and biophysical traits. **i**, Normalized indel percentages in hepatocytes and splenic endothelial cells (ECs) after treatment with siControl of siGFP. *P* value shown, two-tailed *t*-test, average ± s.e.m., $n = 4$. All replicates are biological.

iOligo can be used to reduce hepatocyte editing in models of lung inflammation. We then evaluated whether iOligo could affect gene editing in an established model of acute lung inflammation. Studies have demonstrated that ICAM-2 expression can drive aberrant lung inflammation by recruiting infiltrating immune cells. Compared with wild-type mice, ICAM-2-deficient mice exhibit reduced numbers of lung eosinophils after exposure to inflammatory stimuli[57]. We, therefore, formulated LNP-Hepat carrying iOligo or a scrambled oligonucleotide and injected this intravenously into Cas9 mice. Two hours later, we intravenously injected the mice with LNP-Lung carrying sgICAM-2 (Fig. 6a). Ovalbumin (OVA) was administered to mice (Fig. 6b) to model airway hyper-responsiveness[57,58]. DOPE, 1,2-dioleoyl-sn-glycero-3-phosphoethanolamine.

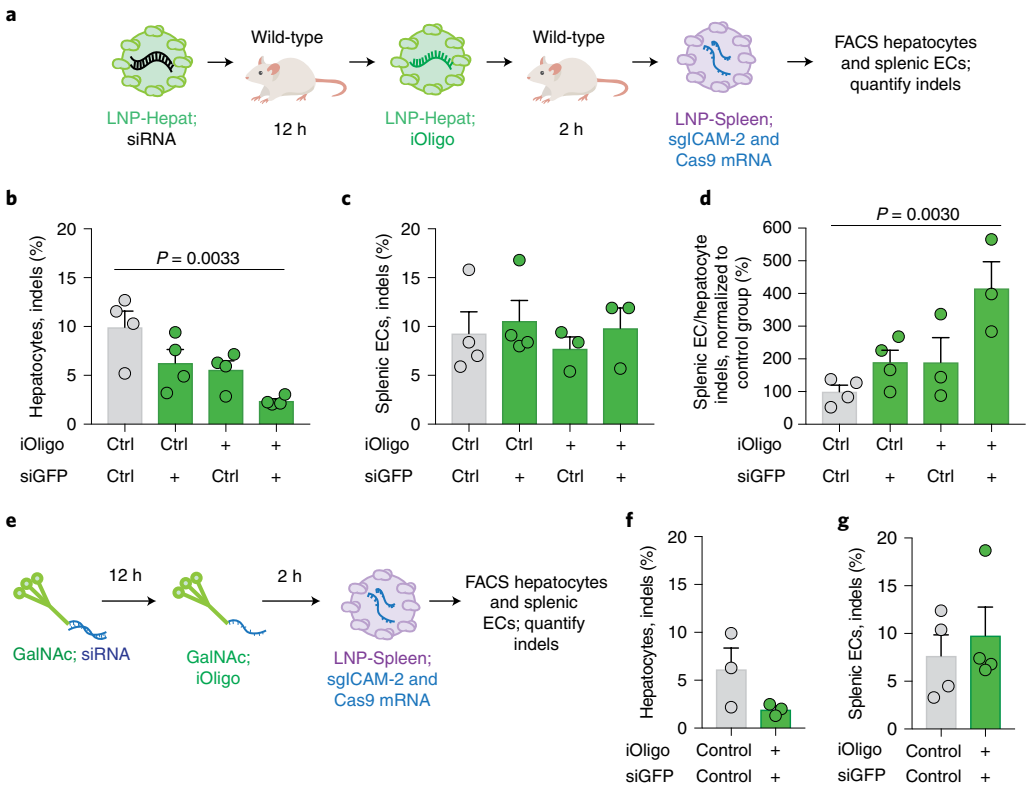

Fig. 5 | Combining iOligo- and siGFP-based approaches markedly reduces cell-type-specific Cas9 gene editing. a, Mice were injected intravenously with LNPs carrying siGFP or siControl; later, mice were injected with iOligo or a scrambled control. The four groups of mice were: siControl/scrambled control, siGFP/scrambled control, siControl/iOligo and siGFP/iOligo. Mice were then injected with LNP-Spleen carrying Cas9 mRNA and sgICAM-2. **b**,**c**, ICAM-2 indel percentages in (**b**) hepatocytes and (**c**) Splenic endothelial cells (ECs) isolated from treated mice. *P* value shown, one-way ANOVA, average ± s.e.m., $n = 3$–4. **d**, The ratio of splenic endothelial cells/liver indels in treated mice. *P* value shown, one-way ANOVA, average ± s.e.m., $n = 3$–4. **e**, iOligo was also delivered subcutaneously using GalNAc in place of LNP-Hepat. Mice were later injected with LNP-Spleen carrying Cas9 mRNA and sgICAM-2. **f**,**g**, The percentage of ICAM-2 indels in hepatocytes (**f**) and splenic endothelial cells after treatment with iOligo and siRNA, average ± s.e.m., $n = 3$–4 (**g**). All replicates are biological. Ctrl, control.

After treatment, we isolated lung and liver tissues. For simplicity, we labelled the conditions as the following: (1) OVA, control iOligo and control sgRNA, (2) OVA, control iOligo and sgICAM-2 and (3) OVA, iOligo and sgICAM-2. We quantified indel percentages in hepatocytes and lung endothelial cells. Compared with mice injected with the control oligo, indel percentages in hepatocytes were reduced by over 60% in iOligo-treated mice (Fig. 6c and Extended Data Fig. 4a). Additionally, ICAM-2 indels in lung endothelial cells increased in mice treated with iOligo (Fig. 6d and Extended Data Fig. 4b). To verify the therapeutic effect, we quantified the percentage of eosinophils, monocytes and neutrophils in lungs using flow cytometry. Compared with the mice treated with controls, OVA treatments led to a 53%, 50% and 82% increase in eosinophils, monocytes and neutrophils, respectively (Fig. 6e,f). In addition, compared with mice treated with only OVA, we observed a decrease in eosinophils (Fig. 6e), monocytes and neutrophils in mice treated with sgICAM-2 (Fig. 6f). Notably, the number of cells decreased back to the baseline established by the control group.

Discussion

We describe evidence that delivering iOligos, siRNAs or combinations thereof can reduce indels in adult mice. We find these data promising, because iOligo and siGFP combinations can be optimized in future work. First, the potency of iOligo might be improved by reducing its length, modifying its sequence or including chemical modifications. Furthermore, the modified Cas9 mRNA could be optimized to reduce off-target editing. Here, we used a Cas9 mRNA with five siGFP-binding sites to reduce Cas9-mediated gene editing; modifications to these binding sites could increase mRNA degradation. Second, we envision enhancing the effect of siRNA by rationally designing a highly potent siRNA to replace the siGFP or, alternatively, using naturally occurring hepatocyte-specific miRNA binding sites. For example, LNP-Hepat has previously been used to silence endogenous genes in hepatocytes at doses below 0.01 mg kg^{-1}. Notably, the dose required to silence an exogenous Cas9 mRNA administered as a large bolus might be higher than the dose required to silence endogenous genes. Third, we think that future studies to fine-tune the relative timing of iOligo and siRNA delivery might further reduce hepatocyte editing. In an ideal case, both the iOligo and siRNA could be delivered as a single GalNAc construct, as was recently reported using two or more siRNAs[59,60].

The biological effect of iOligos could also be improved by selecting different de-targeted genes. For example, in the lung inflammation model, we reduced liver gene editing without reducing lung gene editing. We, therefore, hypothesize that the odds of long-term hepatic side effects resulting from unwanted liver editing decreased as well. Complementing this mechanism, it is foreseeable that de-targeting liver tissues could prevent acute side effects, especially if the targeted gene drives universal cell functions such as lipid metabolism or, alternatively, if the targeted gene is a transcription factor. Finally, given that iOligos interfere with a complex and dynamic process inside the cell (as the mRNA is translated into protein and then interacts with the sgRNA), we think that future studies titrating (1) the ratios of Cas9 mRNA, sgRNA and iOligos,

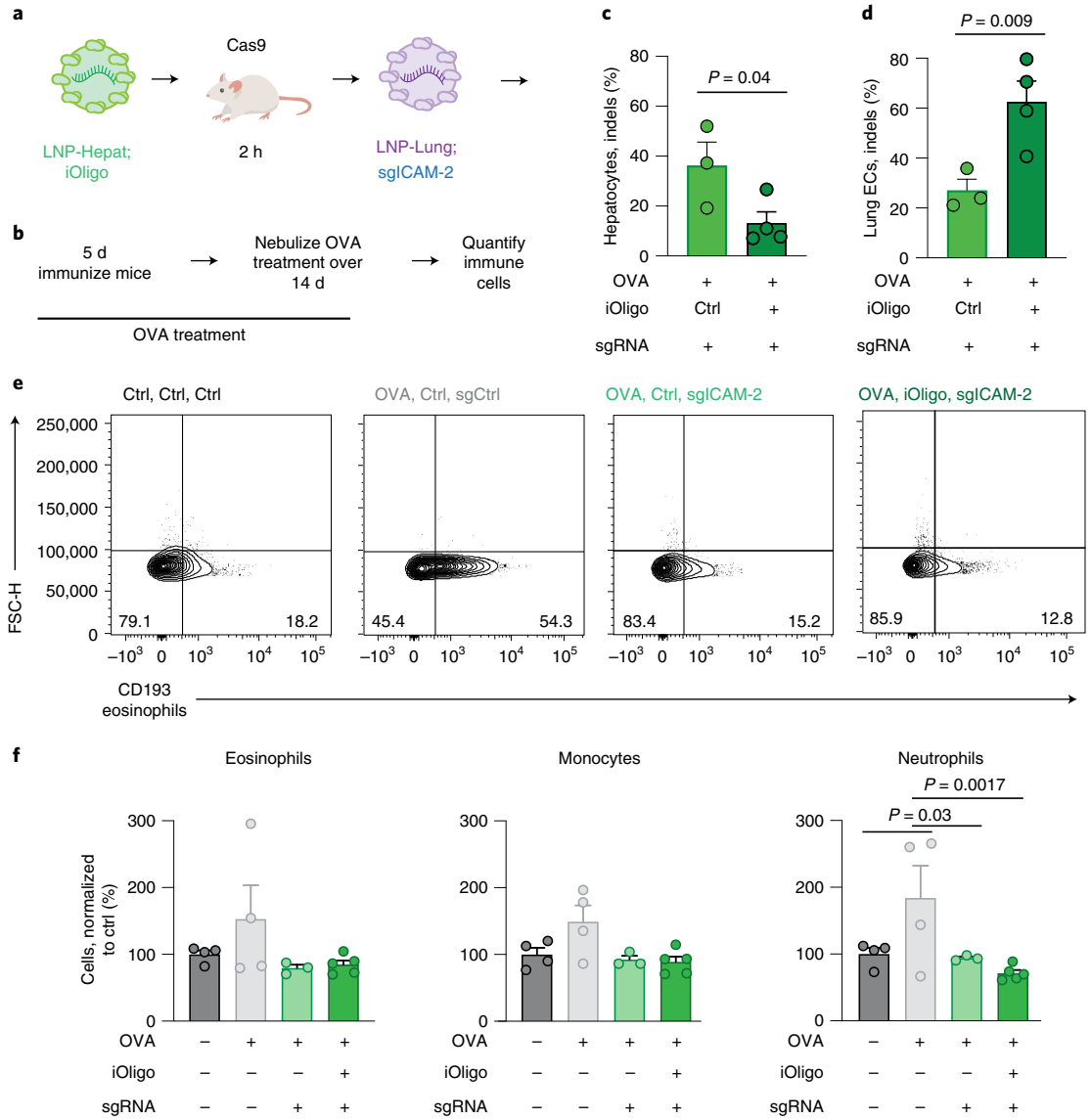

Fig. 6 | iOligo-based approaches reduced cell-type-specific Cas9 gene editing in models of lung inflammation. a, Cas9 mice were injected with LNP-Hepat carrying iOligo or a scrambled control; later, mice were injected with LNP-Lung carrying sgICAM-2. **b**, Mice were then treated with OVA for 21 d. Immune cell infiltration and immune responses in the lungs were quantified. **c**,**d**, The percentage of ICAM-2 indels in hepatocytes (**c**) and lung endothelial cells (**d**) following treatment with OVA, iOligo/Ctrl or sgICAM-2/sgCtrl, *P* values shown, one-way ANOVA, average ± s.e.m., $n = 3$–4. **e**,**f**, The number of eosinophils, monocytes or neutrophils was quantified using flow cytometry for all groups (**e**), and percentage of immune cell subset was normalized to the control group (**f**). The numbers included in the bottom right and bottom left corners of the plots in **e** indicate the percentage of cells that express or don't express CD193, respectively. CD193 is highly expressed on the surface of eosinophils. Coloured text above **e**, corresponds to bar colour in **f**. *P* values shown, two-way ANOVA, average ± s.e.m., $n = 3$–5. All replicates are biological. FSC-H, forward scatter height.

as well as (2) the absolute dose administered, could further reduce unwanted editing. Ideally, these improvements, along with an optimized dosing schedule, may further reduce unwanted hepatocyte gene editing.

Related to these opportunities to further improve this system, we observed that a large overabundance (100-fold) of iOligo was required to disrupt a pre-formed RNP complex. We think that future studies could elucidate whether an optimized system, especially a fully optimized iOligo chemical modification pattern, could reduce this ratio. Regardless, understanding how the iOligo/RNP complex ratio changes as a function of chemical modifications, and whether these relationships are consistent between Cas9 and Cas12a, would provide key insights into the molecular mechanism driving this effect and how this mechanism differs from previously reported anti-CRISPR proteins.

It is important to acknowledge the limitations of this work. First, although iOligo reduced editing in hepatocytes, it did not reduce editing in other tissues. Second, obtaining US Food and Drug Administration (FDA) approval for any treatment that requires multiple drugs is more difficult than obtaining FDA approval for a single drug. However, other anti-CRISPR systems, which would also require administration of the anti-CRISPR as well as the CRISPR itself, are likely being considered for clinical development. Notably, a similar two-injection approach for gene therapies[61] has been successful in phase I and II clinical trials. Third, there is a need for more advanced toxicology assays. We believe that these data

provide a compelling proof of concept, but, as described above, there are several opportunities (iOligo design, siRNA design, timing and stoichiometry) to substantially reduce the overall dose required to achieve this effect. When this fully optimized system is developed, it will be important to perform acute and chronic toxicology studies[62]. Fourth, other approaches can be used to reduce off-target liver activity. Although we show that iOligos can reduce liver editing, improving nanoparticle specificity can also reduce off-target effects. It will be important to continue to develop nanoparticles with improved non-liver tropism.

This work could enable non-hepatocyte Cas9 therapies by removing a critical nanoparticle design criterion. Historically, a nanoparticle would need to deliver Cas9 mRNA and sgRNA exclusively to a new target cell. Now, a nanoparticle that delivers Cas9 mRNA and sgRNA to a desired target cell type and to hepatocytes might be sufficient. We note that we have changed the 'functional tropism' of a previously reported nanoparticle without changing the nanoparticle itself. Given that nanoparticles with activity in non-liver cell types might still accumulate in the liver, this approach may be useful for future RNA therapies.

Methods

Oligonucleotide and siRNA synthesis. iOligos were purchased from Integrated DNA Technologies (IDT). siRNAs (siLuc, siICAM-2, siGFP and hm-siGFP) and sgRNAs (sgGFP and sgICAM-2) were purchased from Axolabs. mRNAs were purchased from TriLink BioTechnologies (GFP and Cas12a) or synthesized as described below (luciferase and SpCas9). Sequences for siRNAs and sgRNAs can be found in Supplementary Figs. 1 and 4.

mRNA synthesis. The Kozak consensus sequence and modified 3′ UTR from murine α-globin was modified using overlap extension PCR and was verified with Sanger sequencing (MWG Eurofins). The sequence of the 3′ UTR is provided in Extended Data Fig. 1a. The DNA template was amplified using the Q5 high-fidelity DNA polymerase (New England Biolabs), purified using the QIAquick PCR purification kit (QIAGEN), digested with the restriction enzyme NOTI to create a 5′ overhang and then purified again. The T7 mScript Standard mRNA Production System was used to generate IVT mRNA (Cellscript) and add a Cap-1 structure and a poly(A) tail. Manufacturer's instructions were followed; the RNeasy Mini Kit (QIAGEN) was used to purify IVT mRNA when necessary. To incorporate modified bases, N1-methylpseudouridine-5′-triphosphate (TriLink BioTechnologies and USB) was replaced in the 25 mM ribonucleotide cocktails. Cytosine triphosphate was purchased from Affymetrix. IVT mRNA was treated with Antarctic Phosphatase (New England Biolabs) for 30 min to remove residual 5′-triphosphates and then purified with the RNeasy kit, quantified using the Nanodrop 2000 (Thermo Fisher Scientific) and stored at −80 °C.

Nanoparticle formulation. Nanoparticles were formulated using a microfluidic device as previously described[43]. In brief, nucleic acids (RNA or DNA) were diluted in QB citrate buffer, pH 3.0, at 10 mM (Teknova), whereas lipid-amine compounds (cKK-E12 and 7C1), alkyl-tailed PEG (C14PEG2000), cholesterol and helper lipids (DOPE and DSPC) were diluted in 100% ethanol. All PEG, cholesterol and helper lipids were purchased from Avanti Lipids. Ratios for each formulation are specified in the Supplementary Fig. 3b. Citrate and ethanol phases were combined in a microfluidic device by syringe pumps. All nanoparticles were dialysed in 20 kD Dialysis Cassettes (Pierce) for 3 h in sterile 1× PBS. Nanoparticles were filtered through a 0.22-µm filter (Foxx Life Sciences). Size and dispersity were measured using dynamic light scattering (DLS, Wyatt Technology). Nanoparticles were considered stable if they were monodisperse and between 20 nm and 200 nm in diameter.

Cell culture. In vitro experiments were performed using iMAECs or IMAECs stably transduced with CAG-SpCas9-EGFP. IMAECs were cultured in EGM-2 Growth Media (Lonza). HEK293 cells were cultured in DMEM/F-12 50/50 media (Corning) supplemented with 10% (v/v) FBS (VWR) and 1% (v/v) penicillin–streptomycin (Thermo Fisher Scientific). Cells were seeded in a 24-well plate at a density of 50,000 cells per well. Sixteen hours after seeding, cells were transfected based on experimental parameters described within the text. In all cases, DNA was isolated using 40 µl of QuickExtract (EpiCentre). DNA for sequencing analysis was isolated using protocols from EpiCentre. All in vitro experiments were done with 4–14 biological replicates per condition.

Animal experiments. All animal experiments were performed in accordance with the Georgia Institute of Technology Physiological Research Laboratory (PRL) animal care and services policy. C57BL/6J (000664) and constitutive SpCas9 (026179) mice were purchased from Jackson Laboratory and used at between 5 weeks and 12 weeks of age. The Georgia Institute of Technology Institutional Animal Care and Use Committee oversaw the ethics of this project. For intravenous injections, rodents were warmed using a heat lamp before injections. For subcutaneous injections, mice were treated under isoflurane anaesthesia. Supplies for animal work were provided by the Georgia Institute of Technology PRL. The nanoparticle concentration was determined using NanoDrop (Thermo Fisher Scientific). All in vivo experiments were done with 3–5 mice per group.

Cell isolation and staining. Cells were isolated 72 h after injection with LNPs unless otherwise noted. Mice were perfused with 20 ml of 1× PBS through the right atrium. Tissues were cut and then placed in a digestive enzyme solution with collagenase type I (Sigma-Aldrich), collagenase XI (Sigma-Aldrich) and hyaluronidase (Sigma-Aldrich) at 37 °C at 550 rpm for 45 min. The digestive enzyme for spleen included collagenase IV. Cell suspension was filtered through a 70-µm mesh-cell strainer, and red blood cells were lysed with red cell lysis buffer (Thermo Fisher Scientific). Cells were stained to identify specific cell populations. The antibody clones used were anti-CD31 (BioLegend, 390) and anti-CD45.2 (BioLegend, 104). We defined the splenic endothelial cell population as $CD31^{+}CD45^{-}$ and the hepatocyte cell population as $CD31^{-}CD45^{-}$, as shown in Supplementary Fig. 9. Antibodies were incubated for 45 min. Next, cells were resuspended in 1× PBS for flow cytometry. Cells were sorted using the BD FacsFusion in the Georgia Institute of Technology Cellular Analysis Core. For in vitro experiments, a BD Accuri C6 was used. Approximately 10^4 cells were isolated per cell type.

Cas12a. Cas12a crRNAs and Cas12a mRNA were designed and generously provided by TriLink BioTechnologies. The Cas12a crRNA targeting GFP was modified with 5 2′F-modified nucleotides on the 3′ end. Cas12a mRNA was codon optimized to be uridine depleted. In brief, HEK293 cells stably expressing d2GFP were seeded at 50,000 cells per well in a 24-well plate. Sixteen hours after seeding, cells were transfected with either scramble or active iOligos with Lipofectamine 2000 (L2K). Four hours after the addition of iOligos, Cas12a crRNA and mRNA were transfected with L2K. After 96 h, DNA was isolated using 40 µl of QuickExtract (EpiCentre).

Cas9 intracellular staining. To determine Cas9 protein translation, the FoxP3/Transcription Factor Staining Buffer kit (Tonbo Biosciences) was used to fix and permeabilize the cells. Anti-Cas9 primary antibody (BioLegend, 7A9) and Alexa Fluor 647 anti-mouse IgG1 (BioLegend, RMG-1) were used to quantify Cas9 protein using a BD Accuri C6 flow cytometer.

TIDE. Indels were measured by TIDE. In brief, an ~600–800-nt amplicon surrounding the sgRNA-binding sequence was amplified using PCR. PCR conditions were 1 min at 95 °C (1 cycle, by 15 s at 95 °C, 15 s at 68 °C, 1 min at 72 °C (40 cycles), followed by a 1 min extension at 72 °C. PCR reactions used HiFi HotStart DNA Polymerase Master Mix (KAPA Biosystems), primers surrounding the region of interest purchased from IDT and water as follows: 1 ul template, 5 ul polymerase master mix, 2 ul water, 1 ul forward primer at 5 nM and 1 ul reverse primer at 5 nM. PCR products were purified and Sanger sequenced by Eton Biosciences.

TIDE requires an input control sequence data file, an experimental sequence data file and the 20-nt sgRNA sequence of interest. The control sequence file was obtained from cells treated with 1× PBS. The sequencing data files were imported into the TIDE software (https://tide.nki.nl/). Parameters used for this study were default settings. First, TIDE aligned the input sgRNA sequence to the control sequence given to identify the expected editing position. Next, an area upstream of the break site is matched between the control sequence and the experimental sequence to determine the difference between the reads. Indels were then determined.

AST enzymatic assay. AST enzymatic assays were performed following manufacturer's instructions to detect abnormal liver function (Abcam, AST kit, ab105135). Livers were isolated 72 h after nanoparticle administration. Homogenized liver tissue samples were used at 1:25 dilutions, and enzymatic activity was measured when colourless probes were converted to coloured/fluorescent products that indicate glutamate produced by AST. Kinetic analyses were conducted at 15-min intervals, and data were analysed according to manufacturer's recommendations.

In vitro luciferase assay. IMAECs were seeded at 10 cells per well in a 96-well plate. Sixteen hours after seeding, cells were transfected with either control (siICAM-2) or active (siGFP) siRNA sequences with L2K. After 8 h, engineered luciferase mRNA was transfected with L2K. Six hours after the addition of the luciferase mRNA, luminescence was measured per manufacturer recommendation using the Promega Bright-Glo Luciferase Assay System.

In vivo luciferase assay. C57BL/6J mice (Jackson Laboratory) were injected with the liver-trophic LNP cKK-E12 carrying either control (siICAM-2) or active (siGFP) siRNA at a dose of 0.5 mg kg^{-1}. After 8 h, mice were dosed with cKK-E12 carrying the engineered luciferase mRNA at a dose of 0.5 mg kg^{-1}. After 6 h,

mice underwent an intraperitoneal injection of CycLuc1. Fifteen minutes after IP administration, mice were euthanized and livers isolated. Isolated livers were deposited in additional CycLuc1 solution and imaged by IVIS. Luminescence was normalized by mouse body weight.

ASGPRL conjugation. The azido-ASGPR-trimer ligand was synthesized as previously described and is detailed in Supplementary Figs. 6–8. To a solution of siGFP-alkyne (1.56 µmol) in nuclease-free water was added a mixture of copper sulfate (8.0 equiv. relative to alkyne, 12.56 µmol, 2.51 µl from a 500 mM stock in water), the copper-binding ligand $(BimC_4A)_3$ (8.0 equiv., 12.56 µmol, 5.02 µl from a 250 mM stock in DMSO), the azido-ASGPR-trimer ligand (1.25 equiv., 1.96 µmol, 9.81 µl from a 20 mM stock in DMSO) and amino guanidine (220 µmol, 22 µl from a 1 M stock in water). A freshly prepared solution of sodium ascorbate (220 µmol, 22 µl from a 1 M stock in water) was added, and then the reaction was gently inverted to mix and incubated at 50 °C for 1 h. The conjugate was purified using a Zeba 7k MW desalting column, followed by ethanol precipitation. The extent of reaction and conjugate purity was determined by electrophoretic analysis and by high-resolution electrospray ionization time-of-flight mass spectrometry.

In vitro Cas9 cleavage activity assays. PCR-amplified ICAM-2 double-stranded DNA (dsDNA); 747 bp) was used as a target DNA substrate. Initial complex formation assembly consisted typically of 1 µM Cas9, 1 µM sgICAM-2 and 1 µM, 3 µM or 100 µM iOligo and was performed in PBS at 37 °C for 10 min. Additional components were added to the complex formation before the digestion reaction was allowed to proceed. The assembled complex was added to 100 nM DNA substrate in the presence of a 10× Cas9 nuclease reaction buffer (200 mM HEPES, 1 M NaCl, 50 mM $MgCl_2$, 1 mM EDTA pH 6.5) and incubated at 37 °C for 60 min. Twenty micrograms proteinase K was added to the reaction before being incubated at 56 °C for 10 min to release the DNA substrate from the Cas9 endonuclease. The reaction was purified with the QIAquick PCR Purification Kit (QIAGEN) following manufacturer's instructions. Digestion products and the fraction of the target cleaved were analysed on a 2100 Bioanalyzer (Agilent).

EMSA. Five-microlitre reactions containing a 5× binding buffer (750 mM KCl, 0.5 mM dithiothreitol, 0.5 mM EDTA, 50 mM Tris pH 7.4) and 1.5 pmol of sgICAM-2 were mixed with and without 1.5 pmol spCas9 protein in the absence or presence of 5 pmol iOligo. Complex formation was performed for 30 min at room temperature before adding 1 µl of loading dye. The samples were run on a 5% tris-borate EDTA (TBE) gel in 1× TBE electrophoresis buffer. After electrophoresis, the gels were visualized with SYBR Green EMSA nucleic acid gel stain.

Mouse model of lung inflammation. To induce a pulmonary inflammatory response, mice were treated with OVA (Thermo Fisher Scientific). All groups were $n = 3$–5. On day 1, mice were treated with an intraperitoneal injection of OVA solubilized in 1× PBS (0.1 mg per mouse). On day 8, animals were treated with 2% OVA in 1× PBS (~1 g per mouse) via nebulization. On days 15–21, animals were exposed to 1% OVA in 1× PBS daily. Mice were loaded into animal restraints (CODA Small Mouse Holder, Kent Scientific), and the nebulizers (Aeroneb, Kent Scientific) were used to aerosolize the OVA treatment. PBS 1× was administered to mice as a negative control. Mice were euthanized on day 21, 3 h after exposure to OVA. Cells were isolated as previously described. The antibody clones used were anti-CD193 (BioLegend, J073E5) for eosinophils, anti-Ly-6G (GR1) (BioLegend, RB6-8C5) for neutrophils and anti-CD11b (BioLegend, M1/70) for monocytes. We defined cell populations as shown in Supplementary Fig. 10.

Reporting Summary. Further information on research design is available in the Nature Research Reporting Summary linked to this article.

Data availability

The main data supporting the results in this study are available within the paper and its Supplementary Information. The raw and analysed datasets generated during the study are too large to be publicly shared, but they are available for research purposes from the corresponding author on reasonable request.

Received: 30 April 2020; Accepted: 11 January 2022;
Published online: 21 February 2022

References

1. Gillmore, J. D. et al. CRISPR–Cas9 in vivo gene editing for transthyretin amyloidosis. *N. Engl. J. Med.* **385**, 493–502 (2021).
2. Porteus, M. H. A new class of medicines through DNA editing. *N. Engl. J. Med.* **380**, 947–959 (2019).
3. Paunovska, K., Loughrey, D. & Dahlman, J. E. Drug delivery systems for RNA therapeutics. *Nat. Rev. Genet.* https://doi.org/10.1038/s41576-021-00439-4 (2022).
4. Lee, B. et al. Nanoparticle delivery of CRISPR into the brain rescues a mouse model of fragile X syndrome from exaggerated repetitive behaviours. *Nat. Biomed. Eng.* **2**, 497–507 (2018).
5. Lee, K. et al. Nanoparticle delivery of Cas9 ribonucleoprotein and donor DNA in vivo induces homology-directed DNA repair. *Nat. Biomed. Eng.* **1**, 889–901 (2017).
6. Gao, X. et al. Treatment of autosomal dominant hearing loss by in vivo delivery of genome editing agents. *Nature* **553**, 217–221 (2018).
7. Miller, J. B. et al. Non-viral CRISPR/Cas gene editing in vitro and in vivo enabled by synthetic nanoparticle co-delivery of Cas9 mRNA and sgRNA. *Angew. Chem. Int. Ed.* **56**, 1059–1063 (2017).
8. Jiang, C. et al. A non-viral CRISPR/Cas9 delivery system for therapeutically targeting HBV DNA and pcsk9 in vivo. *Cell Res.* **27**, 440–443 (2017).
9. Yin, H. et al. Structure-guided chemical modification of guide RNA enables potent non-viral in vivo genome editing. *Nat. Biotechnol.* **35**, 1179–1187 (2017).
10. Finn, J. D. et al. A single administration of CRISPR/Cas9 lipid nanoparticles achieves robust and persistent in vivo genome editing. *Cell Rep.* **22**, 2227–2235 (2018).
11. Rothgangl, T. et al. In vivo adenine base editing of PCSK9 in macaques reduces LDL cholesterol levels. *Nat. Biotechnol.* **39**, 949–957 (2021).
12. Musunuru, K. et al. In vivo CRISPR base editing of PCSK9 durably lowers cholesterol in primates. *Nature* **593**, 429–434 (2021).
13. Zhang, X. et al. Functionalized lipid-like nanoparticles for in vivo mRNA delivery and base editing. *Sci. Adv.* **6**, eabc2315 (2020).
14. Lorenzer, C., Dirin, M., Winkler, A. M., Baumann, V. & Winkler, J. Going beyond the liver: progress and challenges of targeted delivery of siRNA therapeutics. *J. Control. Release* **203**, 1–15 (2015).
15. Semple, S. C. et al. Rational design of cationic lipids for siRNA delivery. *Nat. Biotechnol.* **28**, 172–176 (2010).
16. Dong, Y. et al. Lipopeptide nanoparticles for potent and selective siRNA delivery in rodents and nonhuman primates. *Proc. Natl Acad. Sci. USA* **111**, 3955–3960 (2014).
17. Love, K. T. et al. Lipid-like materials for low-dose, in vivo gene silencing. *Proc. Natl Acad. Sci. USA* **107**, 1864–1869 (2010).
18. Blanco, E., Shen, H. & Ferrari, M. Principles of nanoparticle design for overcoming biological barriers to drug delivery. *Nat. Biotechnol.* **33**, 941–951 (2015).
19. Liu, S. et al. Membrane-destabilizing ionizable phospholipids for organ-selective mRNA delivery and CRISPR–Cas gene editing. *Nat. Mater.* **20**, 701–710 (2021).
20. Cheng, Q. et al. Selective organ targeting (SORT) nanoparticles for tissue-specific mRNA delivery and CRISPR–Cas gene editing. *Nat. Nanotechnol.* **15**, 313–320 (2020).
21. Tsoi, K. M. et al. Mechanism of hard-nanomaterial clearance by the liver. *Nat. Mater.* **15**, 1212–1221 (2016).
22. Zlatev, I. et al. Reversal of siRNA-mediated gene silencing in vivo. *Nat. Biotechnol.* **36**, 509–511 (2018).
23. Landgraf, P. et al. A mammalian microRNA expression atlas based on small RNA library sequencing. *Cell* **129**, 1401–1414 (2007).
24. Lee, J. et al. Tissue-restricted genome editing in vivo specified by microRNA-repressible anti-CRISPR proteins. *RNA* **25**, 1421–1431 (2019).
25. Pawluk, A. et al. Naturally occurring off-switches for CRISPR–Cas9. *Cell* **167**, 1829–1838.e1829 (2016).
26. Shin, J. et al. Disabling Cas9 by an anti-CRISPR DNA mimic. *Sci. Adv.* **3**, e1701620 (2017).
27. Zhu, Y., Zhang, F. & Huang, Z. Structural insights into the inactivation of CRISPR–Cas systems by diverse anti-CRISPR proteins. *BMC Biol.***16**, 32 (2018).
28. Maji, B. et al. A high-throughput platform to identify small-molecule inhibitors of CRISPR–Cas9. *Cell* **177**, 1067–1079.e1019. (2019).
29. Levin, A. A. Treating disease at the RNA level with oligonucleotides. *N. Engl. J. Med.* **380**, 57–70 (2019).
30. Balwani, M. et al. Phase 3 trial of RNAi therapeutic givosiran for acute intermittent porphyria. *N. Engl. J. Med.* **382**, 2289–2301 (2020).
31. Garrelfs, S. LB002ILLUMINATE-A, a phase 3 study of lumasiran, an investigational RNAi therapeutic, in children and adults with primary hyperoxaluria type 1 (PH1). *Nephrol. Dial. Transplant.* **35**, gfaa146. LB002 (2020).
32. Deleavey, G. F. & Damha, M. J. Designing chemically modified oligonucleotides for targeted gene silencing. *Chem. Biol.* **19**, 937–954 (2012).
33. Novobrantseva, T. I. et al. Systemic RNAi-mediated gene silencing in nonhuman primate and rodent myeloid cells. *Mol. Ther. Nucleic Acids* **1**, e4 (2012).
34. Khan, O. F. et al. Endothelial siRNA delivery in nonhuman primates using ionizable low-molecular weight polymeric nanoparticles. *Sci. Adv.* **4**, eaar8409 (2018).
35. Jinek, M. et al. A programmable dual-RNA-guided DNA endonuclease in adaptive bacterial immunity. *Science* **337**, 816–821 (2012).
36. Yildirim, I., Kierzek, E., Kierzek, R. & Schatz, G. C. Interplay of LNA and 2′-*O*-methyl RNA in the structure and thermodynamics of RNA hybrid systems: a molecular dynamics study using the revised AMBER force field and comparison with experimental results. *J. Phys. Chem. B* **118**, 14177–14187 (2014).

37. Ni, C. W., Kumar, S., Ankeny, C. J. & Jo, H. Development of immortalized mouse aortic endothelial cell lines. *Vasc. Cell* **6**, 7 (2014).
38. Sago, C. D. et al. High-throughput in vivo screen of functional mRNA delivery identifies nanoparticles for endothelial cell gene editing. *Proc. Natl Acad. Sci. USA* **115**, E9944–E9952 (2018).
39. Brinkman, E. K., Chen, T., Amendola, M. & van Steensel, B. Easy quantitative assessment of genome editing by sequence trace decomposition. *Nucleic Acids Res.* **42**, e168 (2014).
40. Raper, A. T., Stephenson, A. A. & Suo, Z. Functional insights revealed by the kinetic mechanism of CRISPR/Cas9. *J. Am. Chem. Soc.* **140**, 2971–2984 (2018).
41. Green, A. A., Silver, P. A., Collins, J. J. & Yin, P. Toehold switches: de-novo-designed regulators of gene expression. *Cell* **159**, 925–939 (2014).
42. Zetsche, B. et al. Cpf1 is a single RNA-guided endonuclease of a class 2 CRISPR–Cas system. *Cell* **163**, 759–771 (2015).
43. Li, B. et al. Engineering CRISPR–Cpf1 crRNAs and mRNAs to maximize genome editing efficiency. *Nat. Biomed. Eng.* **1**, 0066 (2017).
44. Zhong, G., Wang, H., Li, Y., Tran, M. H. & Farzan, M. Cpf1 proteins excise CRISPR RNAs from mRNA transcripts in mammalian cells. *Nat. Chem. Biol.* **13**, 839–841 (2017).
45. Li, B. et al. Synthetic oligonucleotides inhibit CRISPR-Cpf1-mediated genome editing. *Cell Rep.* **25**, 3262–3272.e3 (2018).
46. Shen, X. & Corey, D. R. Chemistry, mechanism and clinical status of antisense oligonucleotides and duplex RNAs. *Nucleic Acids Res.* **46**, 1584–1600 (2018).
47. Chen, D. et al. Rapid discovery of potent siRNA-containing lipid nanoparticles enabled by controlled microfluidic formulation. *J. Am. Chem. Soc.* **134**, 6948–6951 (2012).
48. Cullis, P. R. & Hope, M. J. Lipid nanoparticle systems for enabling gene therapies. *Mol. Ther.* **25**, 1467–1475 (2017).
49. Platt, R. J. et al. CRISPR–Cas9 knockin mice for genome editing and cancer modeling. *Cell* **159**, 440–455 (2014).
50. Dahlman, J. E. et al. In vivo endothelial siRNA delivery using polymeric nanoparticles with low molecular weight. *Nat. Nanotechnol.* **9**, 648–655 (2014).
51. Xue, W. et al. Small RNA combination therapy for lung cancer. *Proc. Natl Acad. Sci. USA* **111**, E3553–E3561 (2014).
52. Bartlett, D. W. & Davis, M. E. Insights into the kinetics of siRNA-mediated gene silencing from live-cell and live-animal bioluminescent imaging. *Nucleic Acids Res.* **34**, 322–333 (2006).
53. Hickerson, R. P. et al. Stability study of unmodified siRNA and relevance to clinical use. *Oligonucleotides* **18**, 345–354 (2008).
54. Ray, K. K. et al. Inclisiran in patients at high cardiovascular risk with elevated LDL cholesterol. *N. Engl. J. Med.* **376**, 1430–1440 (2017).
55. Sanhueza, C. A. et al. Efficient liver targeting by polyvalent display of a compact ligand for the asialoglycoprotein receptor. *J. Am. Chem. Soc.* **139**, 3528–3536 (2017).
56. Sehgal, A. et al. An RNAi therapeutic targeting antithrombin to rebalance the coagulation system and promote hemostasis in hemophilia. *Nat. Med.* **21**, 492–497 (2015).
57. Gerwin, N. et al. Prolonged eosinophil accumulation in allergic lung interstitium of ICAM-2 deficient mice results in extended hyperresponsiveness. *Immunity* **10**, 9–19 (1999).
58. Ganzalo, J. A. et al. Mouse eotaxin expression parallels eosinophil accumulation during lung allergic inflammation but it is not restricted to a Th2-type response. *Immunity* **4**, 1–14 (1996).
59. Alterman, J. F. et al. A divalent siRNA chemical scaffold for potent and sustained modulation of gene expression throughout the central nervous system. *Nat. Biotechnol.* **37**, 884–894 (2019).
60. Brown, J. M. et al. Ligand conjugated multimeric siRNAs enable enhanced uptake and multiplexed gene silencing. *Nucleic Acid Ther.* **29**, 239–244 (2019).
61. Kishimoto, T. K. et al. Improving the efficacy and safety of biologic drugs with tolerogenic nanoparticles. *Nat. Nanotechnol.* **11**, 890–899 (2016).
62. Barros, S. A. & Gollob, J. A. Safety profile of RNAi nanomedicines. *Adv. Drug Deliv. Rev.* **64**, 1730–1737 (2012).

Acknowledgements

We thank J. E. Cattie at Emory University and T. E. Shaw.

Author contributions

C.D.S. and J.E.D. conceived the experiments. C.D.S., P.J.S., M.G.F. and J.E.D. designed the experiments. C.D.S., M.P.L., D.L., K.E.L., R.H., B.R.K., S.K., M.S., E.S.E., J.P.F., Z.G., L.G., K.P., C.A.S. and J.E.D. performed the experiments. C.D.S. and J.E.D. wrote the initial draft of the paper, which was edited by all authors.

Competing interests

Patents describing the system documented in this Article have been filed with the US Patent Office. C.D.S. and J.E.D. are listed as inventors on patent (International publication no. WO2021021636A1). C.D.S. works at Beam Therapeutics. J.E.D. consults for GV. All other authors declare no competing interests.

Additional information

Extended data is available for this paper at https://doi.org/10.1038/s41551-022-00847-9.

Supplementary information The online version contains supplementary material available at https://doi.org/10.1038/s41551-022-00847-9.

Correspondence and requests for materials should be addressed to James E. Dahlman.

Peer review information *Nature Biomedical Engineering* thanks Krishanu Saha and the other, anonymous, reviewer(s) for their contribution to the peer review of this work. Peer reviewer reports are available.

Reprints and permissions information is available at www.nature.com/reprints.

Publisher's note Springer Nature remains neutral with regard to jurisdictional claims in published maps and institutional affiliations.

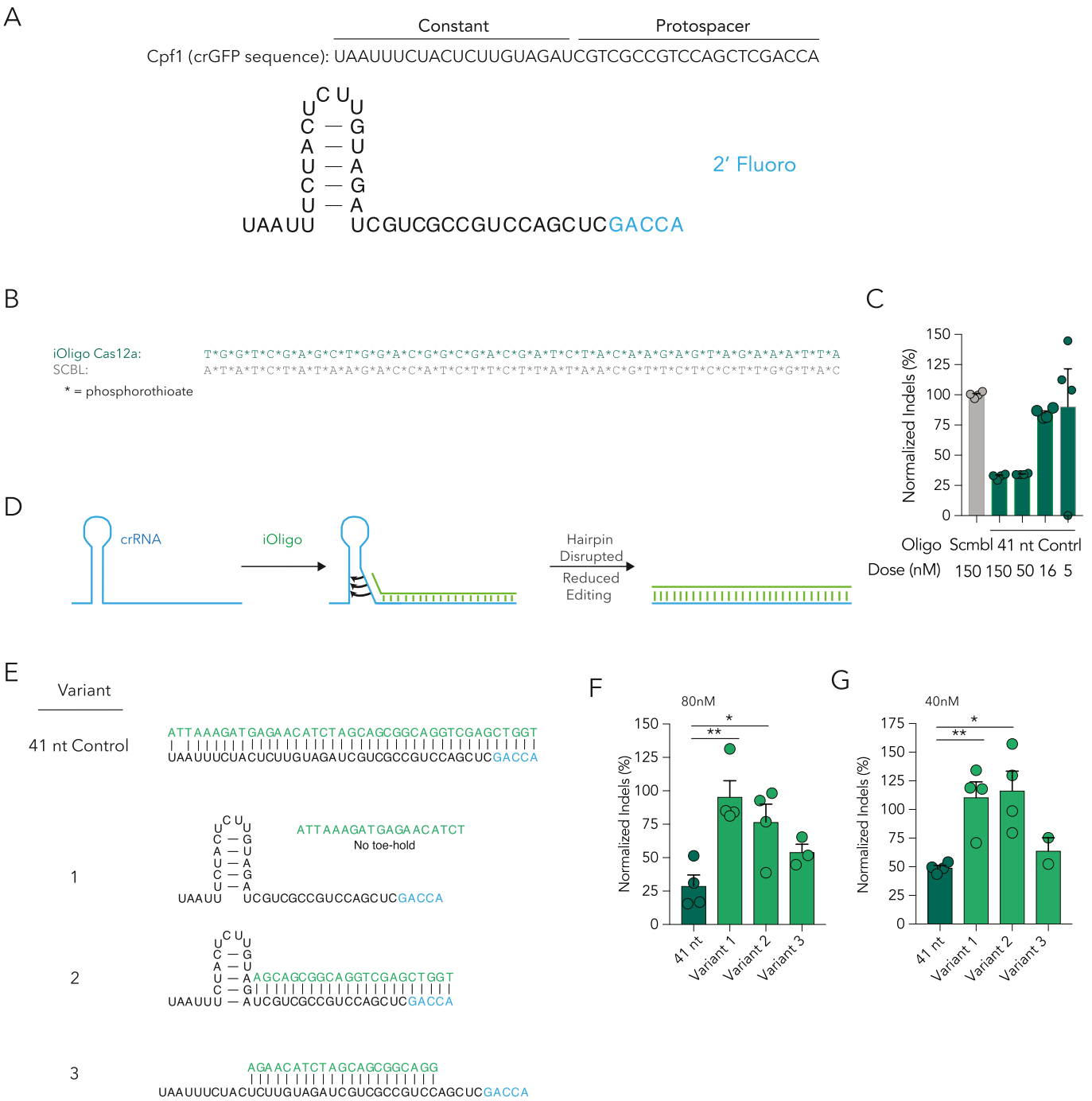

Extended Data Fig. 1 | iOligo variants also inhibit Cas12a-mediated gene editing. (a,b) Sequence and chemical modifications for crGFP and (b) previously reported full-length 41 nucleotide antisense sequence targeting Cas12a. (c) The 41 nucleotide sequence Cas12a reduced indel formation at doses of 150 nM and 50 nM when delivered to cells before crGFP and Cas12a mRNA transfection. (d) Schematic of the proposed toehold mechanism for iOligo targeting Cas12a. The iOligo Cas12a is designed to complement to full- length crGFP RNA, providing the 5′ toe-hold and disrupting RNA secondary structure. (e) The sequences of the truncated iOligo Cas12a, and proposed binding to complementary regions on crGFP. The linear region of the crRNA is required to mediate a strand displacement reaction and facilitate iOligo binding. (F,G) Normalized indels in HEK293T cells after treatment with varying concentrations of full-length and truncated versions of iOligo Cas12a, before crGFP and Cas12a mRNA transfection at (f) 80 nM iOligo, *p = 0.015, **p = 0.008, and (g) 40 nM iOligo, *p = 0.022, **p = 0.0026, one-way ANOVA. All error bars show the average +/- SEM.

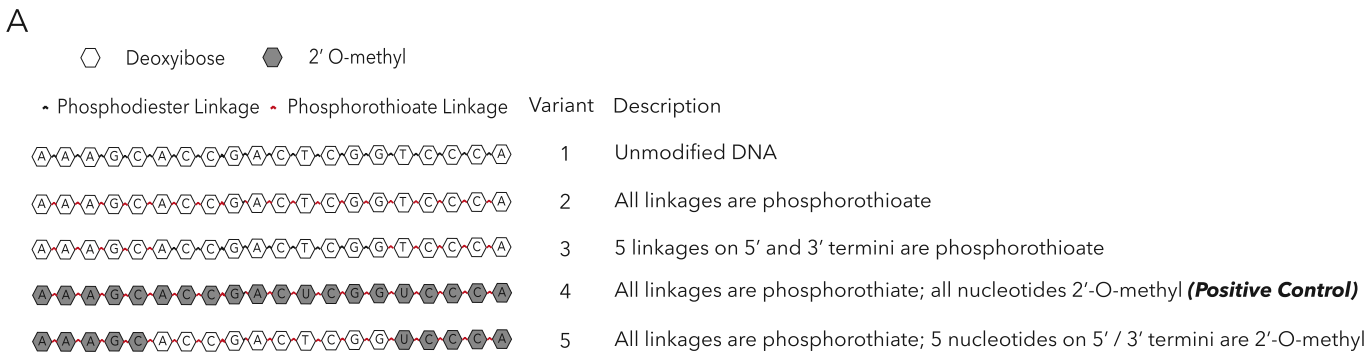

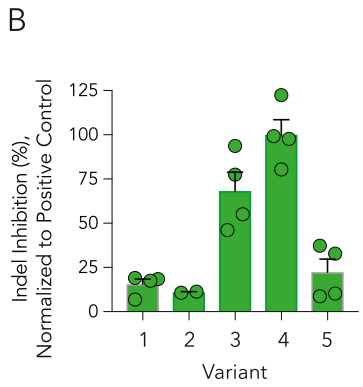

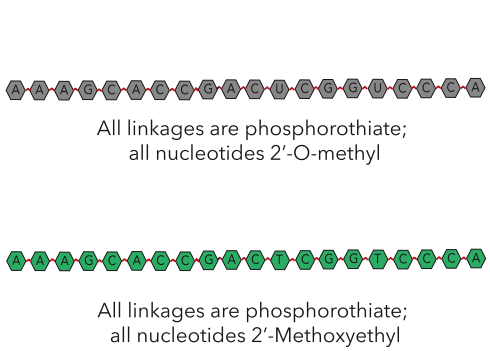

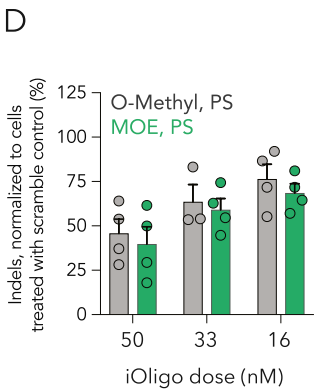

Extended Data Fig. 2 | iOligo chemical modifications affect gene editing. (a) Sequence and chemical modifications patterns for iOligo D with various modification patterns. (b) Normalized indel inhibition of various chemical modification patterns as compared to fully 2′ O-methyl, fully phosphorothioated iOligo-D. (c) Sequence and chemical modifications patterns for iOligo D with 2′ O-methyl and 2′ Methoxyethyl (MOE). (d) Normalized indels of 2′ O-methyl and 2′ Methoxyethyl modified iOligo. All error bars show the average +/- SEM.

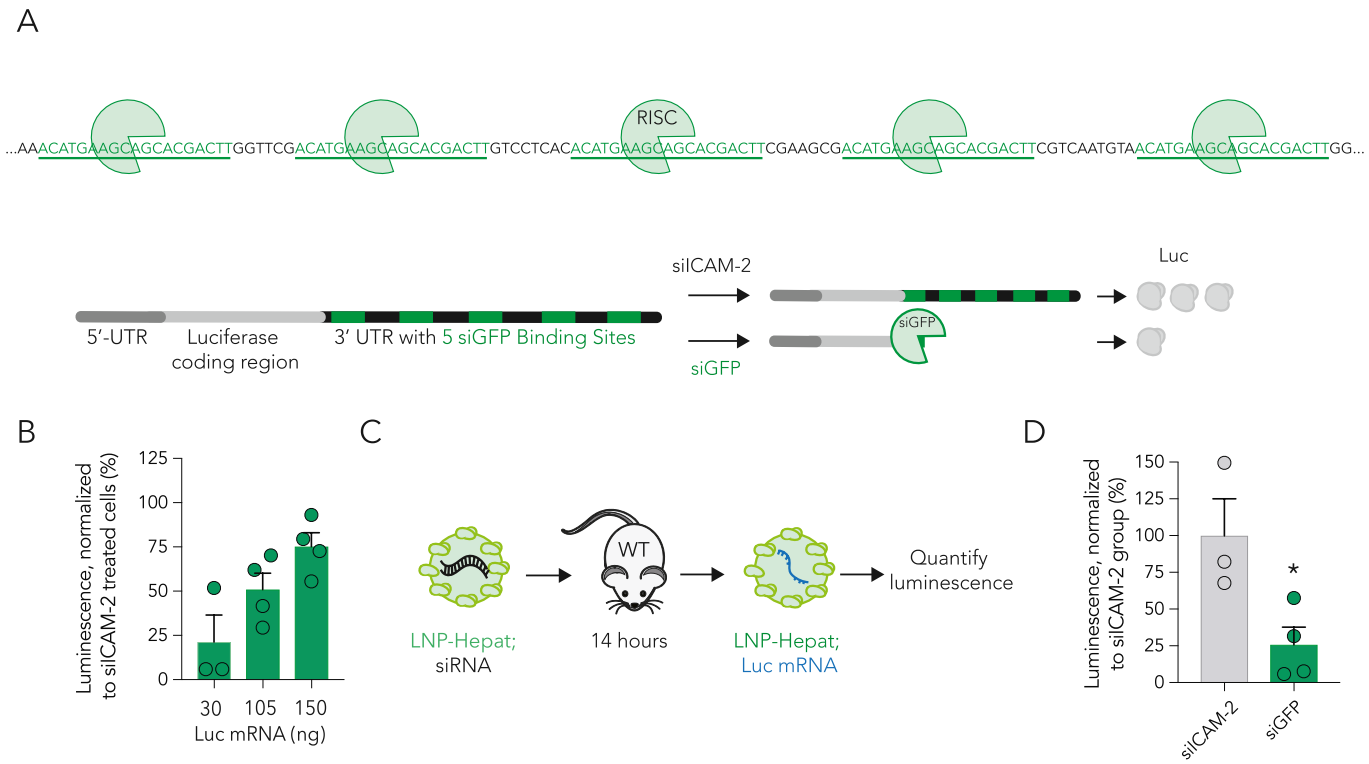

Extended Data Fig. 3 | siRNA-mediated reduction of Cas9 expression controls gene editing in vitro and in vivo. (a) Engineered 3′ UTR with 5 siGFP-binding sites. An engineered luciferase-encoding mRNA with the custom 3′ UTR will be degraded in the presence of siGFP, leading to decreased luciferase protein production as measured by luminescence. (b) The engineered luciferase-encoding mRNA with the custom 3′ UTR led to dose-dependent normalized expression in the presence of siGFP, compared to cells treated with siICAM-2. (c) Mice were pre- treated with either siGFP or siICAM-2 delivered by a hepatocyte-trophic LNP. 14 hours later, the engineered luciferase mRNA was delivered by a hepatocyte LNP. Liver luminescence is measured ex vivo. (d) Normalized ex vivo luminescence the liver from mice pretreated with either siICAM- 2 or siGFP. All error bars show the average +/- SEM.

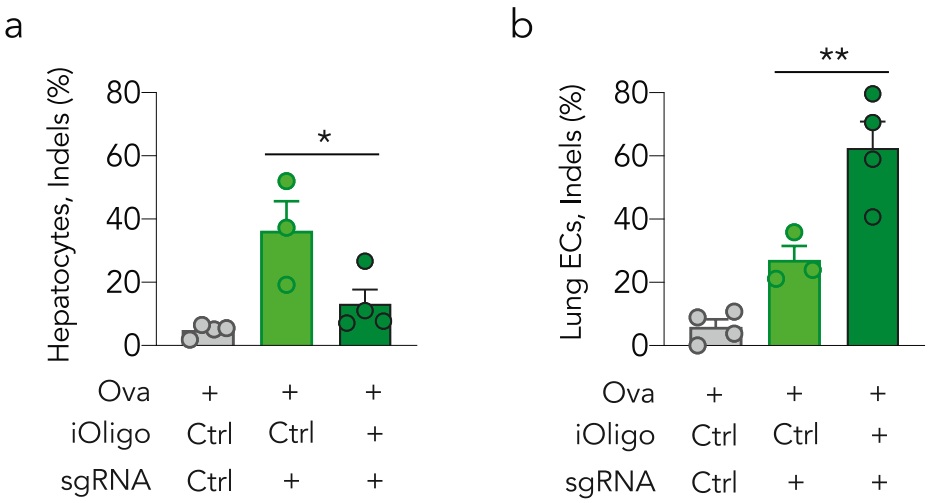

Extended Data Fig. 4 | iOligo-based approaches can be used to reduce cell type-specific Cas9 gene editing in models of lung inflammation. (a) The percentage of ICAM-2 indels in hepatocytes and (b) lung endothelial cells following treatment of Ova, iOligo / Ctrl, and sgICAM-2 / sgCtrl, *p = 0.04, **p = 0.009 one-way ANOVA, average +/- SEM.

nature portfolio

Corresponding author(s): James Dahlman

Last updated by author(s): Jan 11, 2022

Reporting Summary

Nature Portfolio wishes to improve the reproducibility of the work that we publish. This form provides structure for consistency and transparency in reporting. For further information on Nature Portfolio policies, see our Editorial Policies and the Editorial Policy Checklist.

Statistics

For all statistical analyses, confirm that the following items are present in the figure legend, table legend, main text, or Methods section.

n/a	Confirmed
☐	☒ The exact sample size (*n*) for each experimental group/condition, given as a discrete number and unit of measurement
☐	☒ A statement on whether measurements were taken from distinct samples or whether the same sample was measured repeatedly
☐	☒ The statistical test(s) used AND whether they are one- or two-sided *Only common tests should be described solely by name; describe more complex techniques in the Methods section.*
☒	☐ A description of all covariates tested
☐	☒ A description of any assumptions or corrections, such as tests of normality and adjustment for multiple comparisons
☐	☒ A full description of the statistical parameters including central tendency (e.g. means) or other basic estimates (e.g. regression coefficient) AND variation (e.g. standard deviation) or associated estimates of uncertainty (e.g. confidence intervals)
☐	☒ For null hypothesis testing, the test statistic (e.g. *F*, *t*, *r*) with confidence intervals, effect sizes, degrees of freedom and *P* value noted *Give P values as exact values whenever suitable.*
☒	☐ For Bayesian analysis, information on the choice of priors and Markov chain Monte Carlo settings
☒	☐ For hierarchical and complex designs, identification of the appropriate level for tests and full reporting of outcomes
☒	☐ Estimates of effect sizes (e.g. Cohen's *d*, Pearson's *r*), indicating how they were calculated

Our web collection on statistics for biologists contains articles on many of the points above.

Software and code

Policy information about availability of computer code

Data collection	In vivo cell populations were analysed and isolated using the BD FacsFusion in the Georgia Institute of Technology Cellular Analysis Core. Sequencing data were collected with an Illumina NextSeq High Throughput Flow Cell. Luminescence was measured as per the manufacturer's recommendation using the Promega Bright-Glo Luciferase Assay System. In vitro Cas9 cleavage activity assays were analysed on a 2100 Bioanalyzer. AST enzymatic assay was collected on a BioTek Synergy H4 Hybrid Multi-Mode Microplate Reader.
Data analysis	Data were analysed in Graph Pad Prism. The specifics of the data analyses are described in the main text. Flow-cytometry data were analysed using FlowJo. TIDE was used to calculate indel percentages (https:/ /tide.nki.nl).

For manuscripts utilizing custom algorithms or software that are central to the research but not yet described in published literature, software must be made available to editors and reviewers. We strongly encourage code deposition in a community repository (e.g. GitHub). See the Nature Portfolio guidelines for submitting code & software for further information.

Data

Policy information about availability of data

All manuscripts must include a data availability statement. This statement should provide the following information, where applicable:

- Accession codes, unique identifiers, or web links for publicly available datasets
- A description of any restrictions on data availability
- For clinical datasets or third party data, please ensure that the statement adheres to our policy

The main data supporting the results in this study are available within the paper and its Supplementary Information. The raw and analysed datasets generated during the study are too large to be publicly shared, but they are available for research purposes from the corresponding author on reasonable request.

Field-specific reporting

Please select the one below that is the best fit for your research. If you are not sure, read the appropriate sections before making your selection.

☒ Life sciences ☐ Behavioural & social sciences ☐ Ecological, evolutionary & environmental sciences

For a reference copy of the document with all sections, see nature.com/documents/nr-reporting-summary-flat.pdf

Life sciences study design

All studies must disclose on these points even when the disclosure is negative.

Sample size	For the in vitro experiments: n = 4–14 wells of cultured cells in a 24-well plate or group. For the in vivo experiments: n = 3–4 mice per group. The replicates and groups were selected on the basis of the expected variance in the assay readout and of the expected effect of the perturbation.
Data exclusions	No data were excluded.
Replication	In vitro experiments: 4–14. In vivo experiments: 3–4. All attempts at replication were successful.
Randomization	All mice within an experiment were age-matched and strain-matched. All mice were randomized.
Blinding	The authors performing the quantitative measurements and the analyses were not blinded to group allocation.

Reporting for specific materials, systems and methods

We require information from authors about some types of materials, experimental systems and methods used in many studies. Here, indicate whether each material, system or method listed is relevant to your study. If you are not sure if a list item applies to your research, read the appropriate section before selecting a response.

Materials & experimental systems

n/a	Involved in the study
☐	☒ Antibodies
☐	☒ Eukaryotic cell lines
☒	☐ Palaeontology and archaeology
☐	☒ Animals and other organisms
☒	☐ Human research participants
☒	☐ Clinical data
☒	☐ Dual use research of concern

Methods

n/a	Involved in the study
☒	☐ ChIP-seq
☐	☒ Flow cytometry
☒	☐ MRI-based neuroimaging

Antibodies

Antibodies used	anti-CD31 (BioLegend, cat# 102427 clone: 390), anti-CD45.2 (BioLegend, cat# 109806 clone: 104), anti-Cas9 (BioLegend, cat# 844301 clone: 7A9), Alexa Fluor 647 anti-mouse IgG1 (BioLegend, cat# 406618 clone: RMG-1), anti-CD193 (BioLegend, cat# 144517 clone: J073E5), anti-Ly-6G (GR1) (BioLegend, cat# 108408 clone: RB6-8C5), and anti-CD11b (BioLegend, cat# 101208 clone: M1/70). Antibody dilution was typically at 1:200
Validation	anti-CD31 (BioLegend, 390): "Anti-mouse CD31 clones 390 and MEC13.3 bind to their respective non-overlapping epitopes in IgD2 of CD31. CD31 is a 130-140 kD glycoprotein, also known as platelet endothelial cell adhesion molecule (PECAM-1) and EndoCAM". anti-CD45.2 (BioLegend, 104): "CD45.2 is an alloantigen of CD45, expressed by Ly5.2 bearing mouse strains (e.g., A, AKR, BALB/c, CBA/Ca, CBA/J, C3H/He, C57BL, C57BR, C57L, C58, DBA/1, DBA/2, NZB, SWR, 129). CD45, a member of the protein tyrosine phosphatase (PTP) family, is a 180-240 kD glycoprotein expressed on all hematopoietic cells except mature erythrocytes and platelets.". anti-Cas9 and Alexa Fluor 647 anti-mouse IgG1 were used to quantify Cas9 protein. anti-CD193 was used as a marker for eosinophils. anti-Ly-6G was used as a marker for neutrophils. anti-CD11b was used as a marker for monocytes. Each antibody has been validated; the information can be found by searching for (for example) 'BioLegend 390 CD31' or 'BioLegend 104 CD45'.

Eukaryotic cell lines

Policy information about cell lines

Cell line source(s)	We used previously reported cell lines called iMAECs. The original iMAEC report is at https://pubmed.ncbi.nlm.nih.gov/24690145.
Authentication	The cell lines were isolated directly from mice; therefore, there was no reason to authenticate them.

Mycoplasma contamination	The cell lines were not tested for mycoplasma.
Commonly misidentified lines (See ICLAC register)	No misidentified cell lines were used.

Animals and other organisms

Policy information about studies involving animals; ARRIVE guidelines recommended for reporting animal research

Laboratory animals	C57BL/6J (C57BL/6J, 000664) and constitutive SpCas9 (C57BL/6 Cas9, 026179) females between the ages for 5-12 weeks were used in all experiments. They were purchased from Jackson Laboratories. All animals weighed between 17-20 grams. The light cycle of the mouse housing room is from 7 am to 7 pm. Housing rooms are kept at ~ 70 F with ~ 30% average humidity.
Wild animals	The study did not involve wild animals.
Field-collected samples	The study did not involve samples collected from the field.
Ethics oversight	All animal experiments were performed in accordance with the Georgia Institute of Technology's Institutional Animal Care and Use Committee's animal care and services policy.

Note that full information on the approval of the study protocol must also be provided in the manuscript.

Flow Cytometry

Plots

Confirm that:

☒ The axis labels state the marker and fluorochrome used (e.g. CD4-FITC).

☒ The axis scales are clearly visible. Include numbers along axes only for bottom left plot of group (a 'group' is an analysis of identical markers).

☒ All plots are contour plots with outliers or pseudocolor plots.

☒ A numerical value for number of cells or percentage (with statistics) is provided.

Methodology

Sample preparation	Cells were isolated 72 hours after injection with LNPs unless otherwise noted. Mice were perfused with 20 ml of lX PBS through the right atrium. Tissues were finely cut, and then placed in a digestive enzyme solution with Collagenase Type I (Sigma Aldrich), Collagenase XI (Sigma Aldrich) and Hyaluronidase (Sigma Aldrich) at 37C at 550rpm for 45 minutes. The digestive enzyme for spleen included Collagenase IV. Cell suspension was filtered through a 70-μm mesh, and red blood cells were lysed. The antibody clones used: anti-CD31 (Biolegend, 390), anti-CD45.2 (Biolegend, 104). We defined cell populations in the following manner: Splenic endothelial cells (CD31+ CD45–), and hepatocytes (Liver, CD31– CD45–).
Instrument	Cells were stained to identify specific cell populations and sorted using the BD FacsFusion in the Georgia Institute of Technology Cellular Analysis Core. For in vitro experiments, a BD Accuri C6 was used.
Software	We analysed data using FlowJo.
Cell population abundance	Not applicable.
Gating strategy	Live cells were gated on FSC-A/SSC-A, and singlets were identified using FSC-H/FSC-W. Splenic endothelial cells were further defined at CD31+ CD45–, as defined by FMO-gating. Hepatocytes were isolated from live, singlets CD31– CD45– from the liver.

☒ Tick this box to confirm that a figure exemplifying the gating strategy is provided in the Supplementary Information.